DEVELOPMENT OF A MICROFLUIDIC MODULE FOR DNA PURIFICATION VIA PHENOL EXTRACTION

by

MERCEDES C. MORALES

A Thesis submitted to the

Graduate School-New Brunswick

Rutgers, The State University of New Jersey

and

The Graduate School of Biomedical Sciences

University of Medicine and Dentistry of New Jersey

in partial fulfillment of the requirements

for the degree of

Master of Science

Graduate Program in Biomedical Engineering

written under the direction of

Professor Jeffrey D. Zahn

and approved by

_____

_____

_____

_____

New Brunswick, New Jersey

October, 2008

ABSTRACT OF THE THESIS

DEVELOPMENT OF A MICROFLUIDIC MODULE FOR DNA PURIFICATION VIA PHENOL EXTRACTION

By MERCEDES C. MORALES

Thesis Director: Professor Jeffrey D. Zahn

Purification of Deoxyribonucleic acid (DNA) by organic-aqueous liquid extraction, also called phenol extraction, is a standard technique commonly utilized in biology laboratories. In order to minimize interaction energies, membrane components and proteins naturally partition to the organic (phenol) phase while the DNA stays in the aqueous phase, where it can be easily removed. In recent years, microfluidics has become a driving force toward more efficient and autonomous platforms for fluid based diagnostics, chemical reaction chambers, separation and preparation of biological materials.

In this work, the design, fabrication, and performance of long microfluidic devices for DNA extraction are presented. The devices were fabricated using soft lithography to transfer lithographically defined features into a PDMS structure via replica molding. Stratified-flow experiments using a rhodamine dye conjugated bovine serum albumin protein (BSA) in an aqueous phase were conducted to compare different microchannel designs based on their ability to remove proteins from the aqueous phase into the phenol phase. Additionally, the study of BSA partitioning and DNA isolation in a two-phase system under stratified flow condition were addressed, separately and conjunctly. Finally, protein partitioning and DNA recovery were analyzed to evaluate two types of mixing, passive diffusion through stratified flows and droplet enhancement mixing.

ACKNOWLEDGEMENTS

First, I would like to thank Norma Gonzalez and Graciela Abarca at Fulbright Commission in Argentina who believed in my academic potential and my inner strength to success in this study abroad.

I would like to thank next my advisor, Professor Jeffrey Zahn. His mentorship and continuous support have helped me to feel motivated and to enjoy my research. He gave me the opportunity to get involved in stimulating laboratory experiences learning technical skills and inspiring my creativity.

I would like to thank also my former advisor, Professor Fernando Muzzio. It was a great experience for me to work in his group during the first summer at Rutgers University. Fernando's advices have been very useful and I would like to take this opportunity to thank him for his support during my first months at this University.

In the same way, I want to thank Professor Troy Shinbrot for his guidance as Graduate Director and as member of my committee, and Professor Li Cai for granting me access to his equipment and providing helpful comments.

I thank all my colleagues at the Biomedical Engineering Department for making my work in the lab more enjoyable. I would like to specially acknowledge Alex Fok, Larry Sasso and Pantelis Athanasiou, for their support and help with my research.

In addition, I would like to express my sincere appreciation to the faculty and administrative staff at the Biomedical Engineering Department for their advice and help during these years.

Last but not the least I would like to thank my parents and my siblings for their support and encouragement from a distance and all my friends in the United States who make me feel like home.

DEDICATION

To my family and friends for their love, patience and faith in me.

TABLE OF CONTENTS

LIST OF TABLES

LIST OF ILLUSTATIONS

Chapter 1

Introduction

1.1. The need for DNA purification

Since the development of recombinant DNA technology in the 1970's, DNA has been recognized as an important component for biological and biomedical research due to its chemical stability and easy manipulation. As is commonly known, DNA is the blueprint for cellular processes, encoding for proteins and used by cells through RNA transcription and translation to proteins within ribosomes.

There are multiple needs for DNA extraction from complex biological samples. DNA is often purified from cells or tissue lysates, using restriction endonucleases to separate its fragments, and analyzed by gel electrophoresis and southern blotting techniques. There are many research areas where isolation and analysis of DNA plays a central role.

In Agriculture, the discovery of DNA has resulted in tremendous advances to create crops with attributes that they do not have naturally. By manipulating plant genes, agricultural yields have been improved achieving more productivity and pest-resistant varieties.

In Medicine, diagnosis of genetic disorders and gene therapy are the major applications and also the most promising areas of use of DNA techniques. Genetic manipulation has

also allowed the study of many biological processes. Through DNA cutting with restriction endonucleases, DNA insertion into plasmid vectors using DNA ligases, and DNA amplification with polymerase chain reaction (PCR), transgenetic knock out and knock in species, fusion proteins with green fluorescent protein tags and reporter genes have been produced. These manipulations have allowed biomedical researchers to study organism developmental processes, cell cycle regulation, DNA transcription factors among others for studying a range of diseases from cancer development to genetic disorders such as cystic fibrosis.

DNA microarrays, also called GeneChip or Affy chip when an Affymetrix chip is used, are built with thousands of nucleotide sequences of interest attached to a platform in a grid pattern which make it possible to screen multiple sequences at once. DNA microarray technology represents one of the most powerful tools for genome studies and has been used to screen DNA and RNA for many applications such as whole-genome analysis, gene expression analysis and toxicogenomics.

DNA is also a piece of history. The evolution of species can be analyzed by reconstructing gene changes and homology to understand how they evolve. In addition, since mitochondrial DNA is passed on through the maternal lineage, it has been used to trace the migration of humans and to identify bodies with a historical relevance. Use of DNA for identification of people is utilized in forensics for criminal evidence and in paternity disputes through genetic finger printing of specific DNA polymorphisms found in the human genome. A particular and important example of DNA analysis is the development of DNA-based identity test which has recently provided valuable information for identification of missing people during catastrophes or massive attacks,

such as the identification of September 11th victims, and "the disappeareds" and their children in Argentina.

In Defense, DNA analysis is used to detect biological warfare agents and has recently used to trace the anthrax used in the 2001 attacks to a biodefense lab in Fort Detrich, Maryland.

In conclusion, DNA purification is widely used in a very large number of applications which range from daily-life impact areas such as Agriculture, Medicine and Forensics to more general research in Biology, History, Anthropology, and Defense. All these areas of application will be greatly benefited from any advance in DNA preparation by using modern technologies to make the process of isolation, purification and analysis of DNA easier, faster, cheaper and portable.

With recent developments in microfabrication technologies, standard DNA extraction protocols can be improved by using smaller and faster devices which can be integrated with other components such as PCR amplification or capillary electrophoresis separation in a more automatic and compact fashion. In chapter two, the developments in microfluidic devices for DNA extraction are reviewed.

1.2. Standard Bio-Techniques

DNA can be separated and purified by two main methods, by using organic solvents, also called phenol extraction, and by solid-phase-based extraction.

Phenol Extraction

Phenol extraction is an organic-aqueous liquid extraction technique that separates DNA and RNA from cellular components and proteins based on their affinity to the different phases. The procedure consists of digestion of cells or tissue, mixing of the phases where proteins and lipids segregate into the organic phase while DNA stays in the aqueous phase, microcentrifugation, separation and precipitation of DNA with ethanol [1].

Cell lysis is a process of breaking open cells to release the DNA into the solution and leave it accessible. Typical methods include the use of protease enzymes, chemical agent like detergents, or mechanical disruption of cell membranes.

Usually the extraction is prepared in a 1.5 ml microcentrifuge tube and a minimum volume of 100 µl is required for easy manipulation with micropipette tools. The aqueous sample with the lysed cell extract and an equal volume of phenol:chloroform:isoamyl alcohol (25:24:1 v/v) are incorporated into the tube and vortexed vigorously for 5 minutes to mix the phases. During this process, the cell components distribute into either the aqueous phase or the organic phase in order to minimize interaction energies. The cell membrane lipid components and proteins will partition to the organic phase and DNA will stay in the aqueous phase due to its polar nature having greater affinity to the aqueous phase. The separation occurs at the organic-aqueous interface. Increasing the interfacial interaction area is central to maximize the effective partitioning. In macroscopic systems this is accomplished through the vortex mixing.

Following partitioning, centrifugation is the next step to separate the two phases by density differences. The aqueous phase, the upper one in the tube due to its lower density,

is now removed with a micropipette tool. This extraction and centrifugation process can be repeated to remove more components and to completely separate the phases.

The aqueous phase is then mixed with 2.5 volumes of ice cold 100% ethanol, and microcentrifuged at high speed which precipitates the DNA into a pellet. The supernatant solution is removed. Finally, 70%-80% ethanol is added, mixed and discarded to wash the remaining pellet removing excess salts. After washing, the DNA is resuspended in 50-100 µl of Tris-EDTA (TE) buffer.

Solid Phase Extraction (SPE)

This technique is based on the absorption of DNA onto a silica solid phase under high salt concentration condition to separate DNA from the cell components. Many purification kits are commercially available (e.g. Qiagen, Promega, Biorad, Epicentre). Commercial kits usually utilize solid phases like silica gel, glass matrix, or membranes to bind and purify DNA. The main steps for solid phase extraction are lysis of the cells, absorption of DNA, washing, and elution of DNA [2].

Cell lysis is done under alkaline conditions and the solution is then loaded into the purification kit which consists of a packed silica column. In presence of high salt concentration, the DNA binds to silica because of electrostatic shielding between the DNA and the silica surface while the other cell components do not.

After the DNA adsorption, a washing step is required to remove proteins and other contaminants from the column. The purified DNA is then recovered via the introduction

of an elution buffer at low salt concentration which will promote the detachment of the DNA molecules.

This technique does not have the inconvenience of dealing with organic solvents like the previous method. Pure DNA is ready for immediate use without requirements of desalting or precipitation steps. However, the extraction efficiency obtained with this technique is lower than the phenol extraction-ethanol precipitation procedure and is more susceptible to protein contamination.

1.3. Thesis Overview

This work describes the design, fabrication, and performance of long microfluidic devices used as platform for diffusive DNA extraction by organic solvents. The main aims are to quantify protein partitioning between the aqueous and the organic phase and DNA purification within the device, and to evaluate two modes of extraction, passive diffusion through stratified flows and droplet enhancement extraction.

In chapter one, an introduction to DNA extraction is provided. The necessity of DNA isolation is addressed first to understand the importance and relevance of the investigation. A brief description of standard bio-techniques is also provided.

The second chapter presents an overview of the microfluidic field and a state-of-art review of recent research towards DNA extraction chips.

The third chapter introduces the theoretical framework which is the basis of this work. Two-phase systems in microfluidic devices are described, considering the forces and

factors implicated in this behavior. The partitioning mechanism is also briefly addressed. Lastly, different mixing methods to achieve protein partition are described.

Chapter four examines the criteria used to design the serpentine device, the fabrication process and the materials used in the experiments. Measurement methods are also described in this chapter as an introduction to the experiment results.

Chapter four presents the results obtained from the experiments. A comparison between different devices was done using the measurement methods described in chapter three. Protein partitioning and DNA purification were analyzed for stratified flows and droplet-based flows in this section.

In chapter five the results are summarized and discussed and finally the last chapter of this thesis addresses future prospects for improving this research.

Chapter 2

Background and Recent Developments

2.1. The Microfluidics Revolution

Microfluidics is defined as the study and application of fluid flow at the micro scale. With the reduction of scale sizes to micrometers, the fluid physics changes dramatically establishing an entirely new field, microfluidics. Inspired by the microfabricated-integrated-circuit revolution, microfluidics has begun to change how biology, chemistry and biomedical research are conducted [3-6]. The possibility of automation of complex, laborious chemical and biological process is now real [5]. In medicine, the fact of working with very small volumes makes this technique very attractive for rapid, low cost diagnosis based on screening of body fluids [5]. One proof of the importance of development of microfluidic devices is the high number of papers written in the last years in this area [3].

What makes microfluidics so attractive? First at all, the reduction of scale leads to optimization of chemical reactions requiring lower volumes of expensive reactants. Down-scaling also increases the surface area to volume ratio which is a tremendous advantage for interfacial-based processes [3, 5].

One distinctive feature of microflows is that they are laminar flows; therefore, turbulence is not present. Under this condition, mixing is done by diffusion. The Péclet number (Pe) which relates the convective transport and the transverse diffusion is usually very large in these systems. The number of channel widths required for particles to diffuse across the entire channel varies linearly with Pe. Therefore, full mixing by diffusion in these systems implies the need of longer devices [6].

In microfluidics, the flow behavior is influenced by viscosity rather than inertia. Viscous forces play a very significant role and can be used to alter the fluid behavior. In the same way, wetting and interfacial properties, usually neglected in the macroscale, are extremely important in this field and have been used for different applications in chemistry and biology [3, 4, 7-10].

In biology and chemistry, the most exciting feature of microfluidics is the possibility of automation and integration of several processes in one chip which is known as Lab-on-a-chip or micro total analysis systems (μTAS) technology. This characteristic reduces the individual user manipulation steps diminishing the risk of contamination. Finally, other possible attributes of this technology are portability, low-cost and disposability which are key features for medical diagnostics.

2.2. Microfluidic Research in DNA extraction

Microfluidic approaches are the cutting-edge for automation and optimization of traditional analytical processes and point-of-care medical systems. For this reason, integrating cell lysis, purification, amplification and analysis of nucleic acids into a

micrototal analytical system (μTAS) represents the driving goal of many research groups all over the world [11-20]. Advances in microfluidics as well as in material sciences have made possible to rethink standard DNA purification procedures, using the attractive characteristics of microfluidic chips to provide simplicity, automation, and reduction in time, reagents and user handling.

To date, the research into DNA purification has been mainly focused to scale down the solid phase extraction technique rather than the standard phenol extraction. Principally motivated by the advances in μTAS, many research groups have developed systems to make real the possibility of integration of multiple DNA handling processes in a simple microchip [11-20]. Some of their work is reviewed here:

Cepheid Inc.

This team has been working in the development of a cartridge where lysed cells are introduced and DNA purification and Polymerase Chain Reaction (PCR) amplification occur inside of the device [13, 21]. The DNA extraction chip consists of silicon pillars, made by deep reactive ion etching (DRIE), to which DNA binds (Fig. 2.1a). The use of these columns increases the surface area to volume ratio, providing a high binding capacity which is approximately 40 ng/cm^2. Rapid, PCR thermal cycles are incorporated to the chip to amplify DNA quantities in cases of low concentration samples. Washing and elution step are all incorporated into the chip. The integrated cartridge with the different process chambers is shown in Fig. 2.1b. The extraction efficiency was found about 50 % using bacteriophage λ DNA as the target and DNA extraction was successful with both low and high concentrations of DNA samples (100-1000 ng/ml).

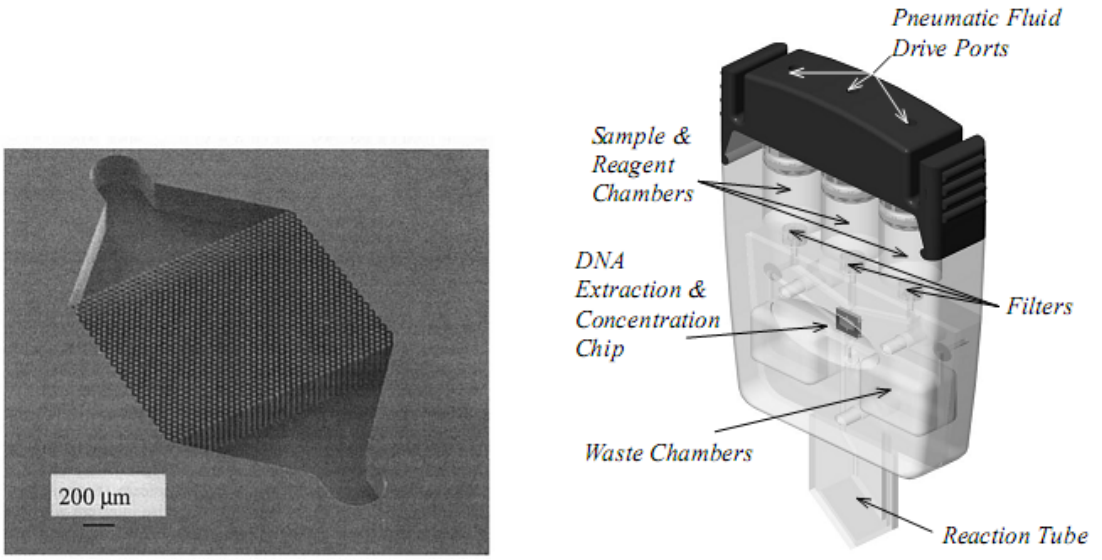

a b

Figure 2.1. a) DNA extraction chip. b) Integrated microfluidic cartridge containing the DNA chip and PCR reaction tube. Images taken from [13, 21].

Landers's group

In this case, the micro solid-phase extraction (µSPE) method was based on silica beads immobilized within a sol-gel instead of silicon or glass pillars like the previous groups [11]. Beads packed in the microfluidic device increase the absorption area where DNA will bind. The channel is first loaded with the beads and then filled with sol-gel to immobilize the silica particles (Fig. 2.2C). In addition, to keep the beads trapped in the device, the gel helps keep them separated, avoiding clogging, and increases the effective absorption surface area. The chip consists of a simple channel as shown in Fig. 2.2A. It requires an outside lysis step and externally loading of sample, washing buffer, and elution buffer. This device was tested with blood and bacterial samples and has

demonstrated an extraction efficiency of 50% for human genomic DNA and 70% for λ DNA.

In recent years, this group has developed a glass microdevice which combines silica bead-based extraction with PCR on a single chip [22], as well as a two-stage device that use a reversed-phase and a monolith in series to improve the DNA extraction efficiency [23], and a fully integrated device which receives crude biological sample and performances DNA extraction, PCR amplification and electrophoretic separation inside the device [24].

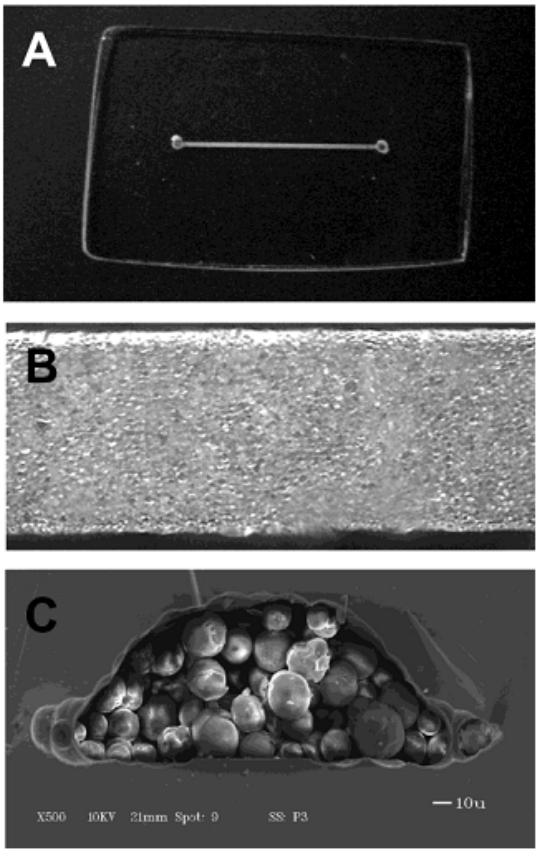

Figure 2.2. Silica particle-based microchip with sol-gel immobilization. A) 1x magnification; B) 10x magnification; C) 500x magnification of cross section. Image taken from [11].

Quake's group (2004)

The microfluidic device developed by this group was fabricated using soft lithography techniques and all the processes involved in the purification of nucleic acids were integrated in one chip (Fig 2.3) [14]. By external pneumatic activation, valves can control the traffic of the different buffers and samples to the corresponding chamber, and isolate units from the rest of the chip. The main units are lysis buffer chamber, dilution chamber, and cell chamber. In addition, this microfluidic device was designed with a parallel architecture to process different samples in parallel at the same time. In Fig 2.3 a-e, the DNA purification process is shown. Cell sample, dilution buffer and lysis buffer are introduced first into the device and pumped through a rotary mixer which is also controlled by hydraulic valves that constantly open and close the entrance of fluids. The function of this step is to mix the components and reduce the time taken for lysis of the cells. Then, the mixture is flushed over beads which are preloaded in the device. DNA binds the beads and a washing buffer is used to flush the waste. Finally, the elution buffer is added and DNA is collected. In this fully automatic fashion, DNA extraction can be performed with a very little user handling.

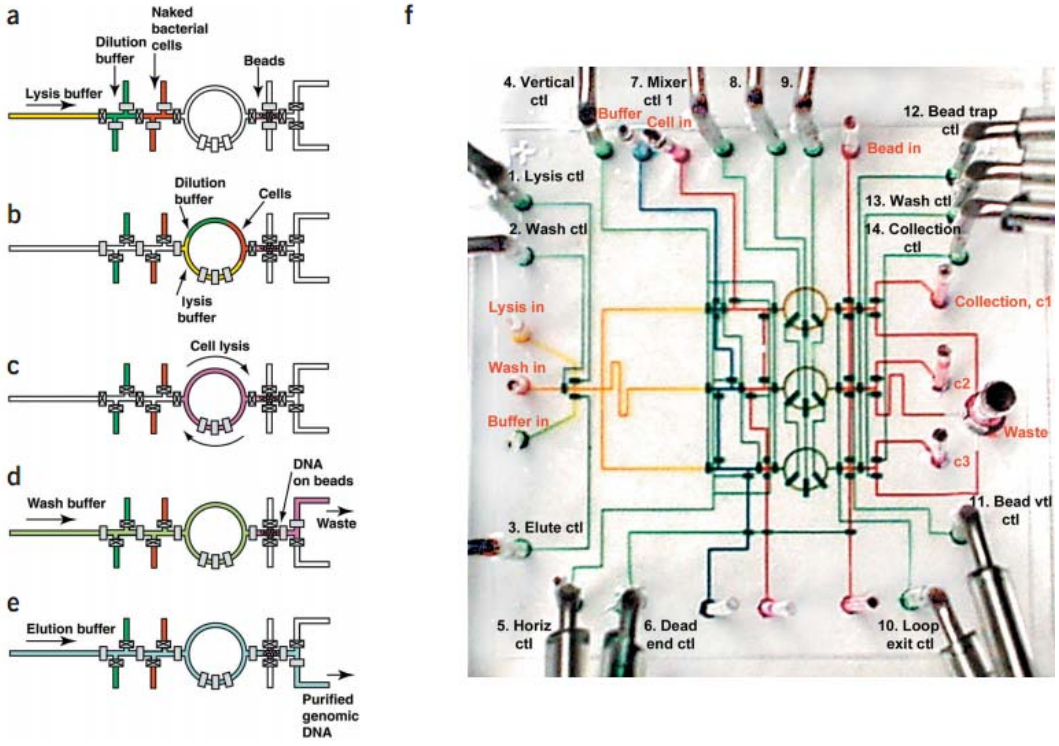

Figure 2.3.a-e Schematic diagram of the DNA purification process. f) Image of the DNA microfluidic chip with parallel architecture. Image taken from [14].

Liu's group (2007)

This team has developed a novel microfluidic chip which performs cell lysis and DNA purification in the same platform in a continuous manner (Fig. 2.4) [15]. The lysis is made by mixing the cell samples with lysis buffer using a sandwich-type mixing model and a serpentine channel configuration to enhance mixing. The DNA absorption is done in a porous silicon surface (Fig. 2.5), where the surface area to volume ratio is approximately $300m^2/cm^3$. The device was tested with genomic DNA and the resulting recovery was 83%. In addition these advantages, the whole process, lysis and

purification, can be achieved within 20 min. Finally, this biochip has great potential to be integrated with PCR modules.

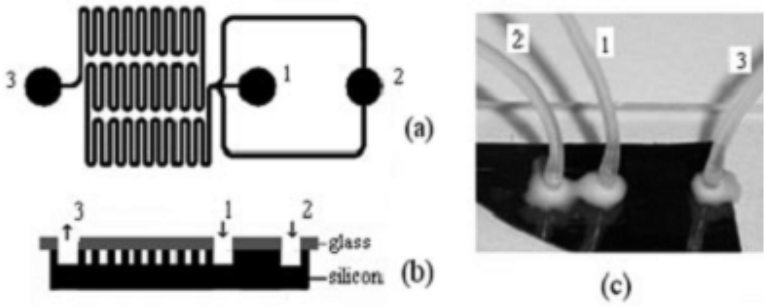

Figure 2.4. a) Schematic top view; b) cross view; c) photograph of the chip. (1) cell inlet, (2)buffer inlet, (3) outlet. Image taken from [15].

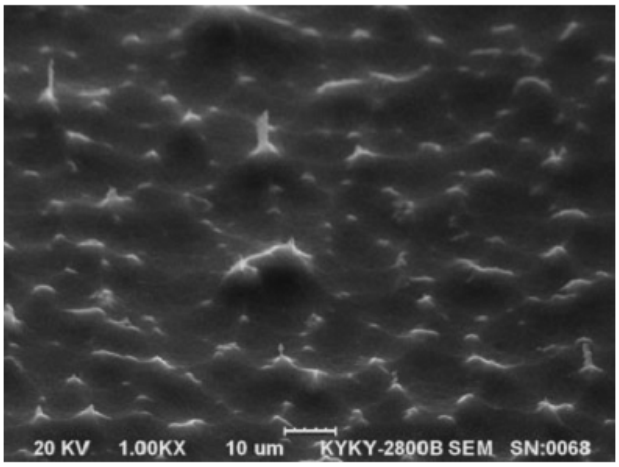

Figure 2.5. SEM of porous silicon used as solid-phase. Image taken from [15]

Klapperich's group (2007)

This group developed a plastic platform for viral RNA extraction [17]. The solid-phase extraction system was formed by silica particles trapped with a porous polymer monolith

(Fig. 2.6). The microfluidic chip was made of medical grade cyclic polyolefin by hot-embossing with a master mold, separated and thermally bonded. The silica microbeads are trapped in the channel by in situ photopolymerization through outside of the device in a porous polymer monolith. The proposed chip presents the advantages of low cost, mass production potential, disposable, easy-to-use and minimal user handling.

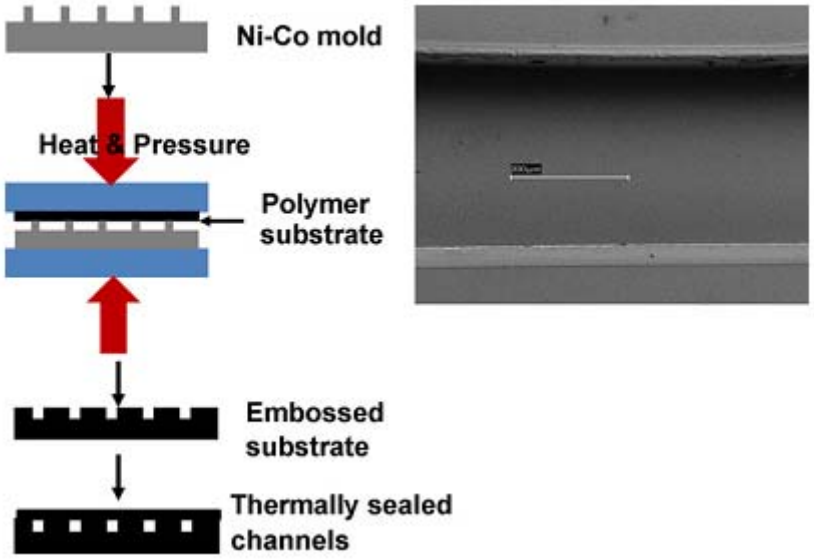

Figure 2.6. Fabrication step and micrograph of the disposable microfluidic chip. Image taken from [17]

Zahn's group

First steps towards a miniaturized portable chip for phenol extraction were taken by this group [18-20]. Analysis of two-phase behavior using phenol and aqueous solution and stabilization of the interface were made as the first approach to the problem [19]. Furthermore, computational and experimental analysis of droplet formation enhancement was presented as a proposed mixing procedure for rapid DNA extraction [18]. Mixing between phases using electrohydrodynamic (EHD) instabilities was also investigated

analytically and experimentally to increase the surface area where partitioning occurs (Fig. 2.7) [20].

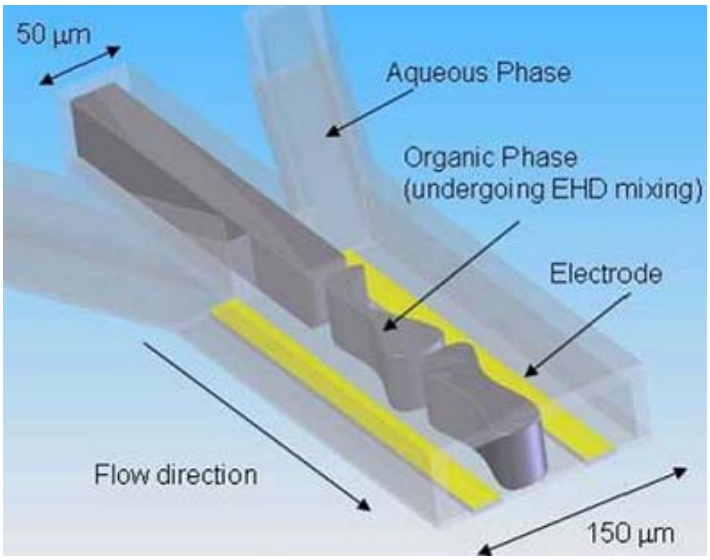

Figure 2.7. Schematic of three inlet device with electrohydrodynamic mixing. Image taken from [20].

This thesis is a compilation of advances made in the development of DNA extraction platform of Zahn's group. Based on the previous results [18-20], the main objectives were the quantification of protein partitioning and DNA purification efficiency of the device, and the evaluation of different types of mixing.

In the next chapter, the theory behind the experiment is presented to provide the transport phenomena background which will allow a better understanding of the device's design and the experimental results.

Chapter 3

Theory

3.1. Two-Phase Microfluidic Systems

Multiphase flow is defined as two or more different immiscible fluids present in a system. Multiphase flows are complex systems but they have several attractive characteristics which make them very practical for applications in microfluidics [9]. In the last years, many reviews have been written on this topic summarizing the multiphase fluid behavior, methods of control for both droplet-based and stratified flows, pumping principles, and several applications [7-10, 25, 26].

The description of fluid dynamics at small scales is quite different if it is compared to large-volume systems [6]. Assuming conditions of constant density ρ and viscosity μ and incorporating the interfacial effects σ, the equations that describe the fluid physics in the two bulk fluids are the Navier-Stokes equations and the continuity equation:

$$\rho\left(\frac{\partial \boldsymbol{u}}{\partial t}+\boldsymbol{u}\cdot\nabla\boldsymbol{u}\right)=-\nabla p+\mu\nabla^2\boldsymbol{u}+\boldsymbol{f} \tag{3.1}$$

$$\nabla\cdot\boldsymbol{u}=0 \tag{3.2}$$

where u is the velocity of the fluid, p is the pressure and f represents body force density.

In microfluidic devices, inertial forces are small compared to viscous forces and the nonlinear term in (3.1) can be neglected, leaving the Stokes equation [6, 9]:

$$\rho\left(\frac{\partial \boldsymbol{u}}{\partial t}\right) = -\nabla p + \mu\nabla^2 \boldsymbol{u} + \boldsymbol{f} \tag{3.3}$$

In this work the driving force is always pressure but other type of external forces can be applied to microfluidics such as electrical, magnetic and thermal [3, 6].

In addition, the force equilibrium condition at some arbitrary surface element A at the interface requires that

$$\iint_A (\boldsymbol{T} - \hat{\boldsymbol{T}}) \cdot \boldsymbol{n} dA + \int_C \gamma \boldsymbol{t} dl = 0 \tag{3.4}$$

where $\boldsymbol{T}$ and $\hat{\boldsymbol{T}}$ are total bulk stress in the flow above and under the surface element A, respectively, n is the unit vector normal to the interface, γ is the interfacial tension, and t is the unit vector tangential to the interface and normal to the boundary curve C.

Applying Stokes's theorem to (3.4) and considering an arbitrary surface element A, it follows that

$$(\boldsymbol{T} - \hat{\boldsymbol{T}}) \cdot \boldsymbol{n} + grad\ \gamma - \gamma \boldsymbol{n}(\nabla \cdot \boldsymbol{n}) = 0 \tag{3.5}$$

To obtain the normal stress balance, inner product is applied to (3.5) and T is replaced by $\boldsymbol{T}_{ij} = -p\boldsymbol{\delta}_{ij} + \boldsymbol{\tau}_{ij}$ where p is pressure and τ is the shear stress component $\boldsymbol{\tau}_{ij} = \mu\left(\frac{\partial \boldsymbol{u}_j}{\partial x_i} + \frac{\partial \boldsymbol{u}_i}{\partial x_j}\right)$, this gives

$$(\hat{p}_{tot} - p_{tot}) + [((\boldsymbol{\tau} - \hat{\boldsymbol{\tau}}) \cdot \boldsymbol{n}) \cdot \boldsymbol{n}] - \gamma(\nabla \cdot \boldsymbol{n}) = 0 \tag{3.6}$$

Eq. 3.6 states the relationship between pressure, shear stress, interfacial tension and curvature. The changes of interface curvature compensate for the differences in pressure and shear stress in both bulk phases to maintain the stress equilibrium at the interface.

The same way, the tangential stress component can be obtained by taking the inner product of (3.5) with the unit tangent vector t, that is

$$((\boldsymbol{\tau} - \hat{\boldsymbol{\tau}}) \cdot \boldsymbol{n}) \cdot \boldsymbol{t} + (grad\, \gamma) \cdot \boldsymbol{t} = 0 \tag{3.7}$$

From (3.7), nonzero interfacial tension gradient can drive motion of fluid and, conversely, shear stress can induce no uniform interfacial tension at the surface. These motions are know as Marangoni flows. However, in this work the interfacial tension was considered uniform across the interface.

The fluid dynamic can be characterized by dimensionless numbers which relate the competition between different forces. In Squires and Quake's review [6], a complete list of dimensionless number used in microfluidics is shown. However, if we consider the following forces: buoyancy, gravitational, inertial, viscous and interfacial forces, the importance of each force will dramatically change as the scale goes from macro to microscale. In microfluidics, buoyancy, gravitational and inertial forces become less important and can be neglected. On the other hand, viscous and interfacial forces, usually ignored in the macroscale, become very important to explain the fluid behavior in microchannels [9].

Reynolds number is the most representative number to characterize microfluidic flows and it is the ratio between inertial and viscous forces:

$$\mathrm{Re} = \frac{\rho U L}{\mu} \tag{3.4}$$

where U is the average flow velocity and L is the characteristic flow dimension [3]. In microscales, Re for liquid flows in usually between the order of 10 and 10^{-4} [9]. Therefore, the inertial forces can be ignored and only laminar flow is expected. In addition, in simple channels and pressure-driven flows the velocity profiles are parabolic. More about fluids under low-Re-number conditions can be found in the literature [27, 28].

In multiphase systems, the capillary number is the most significant dimensionless number. It relates the viscous forces which act tangential to the interface elongating it and the interfacial forces which act normal to the interface minimizing the interfacial area by inducing droplet formation [19]. The capillary number can be expressed as:

$$Ca = \frac{\mu U}{\gamma} \tag{3.5}$$

If the viscous forces are more significant than the interfacial forces, the multiphase flow behavior is parallel or stratified (Ca>>1). Segmented or droplet-based flow occurs when interfacial forces are predominant (Ca<<1). Other regimes appear in the transition such as pearl-necklace and pears regimes [29, 30]. The analysis of multiphase flow behavior has been done in channel configuration like T, Y and cross configuration [9].

Multiphase flow pattern are influenced by multiple factors. The fluid behavior depends on interfacial forces between the fluids and channel walls, individual fluid viscosities, fluid velocities, and the geometric characteristics of the channel [29, 31-33].

First, interfacial forces can be altered using surfactants which will stabilize the interface due to the reduction of the interface tension [19]. Wall surface treatment, guide-structure microchannels and self assembled monolayer modifications are other methods to control flow behavior in microchannels [34-36].

Second, viscosity can be chosen to influence flow patterns in a desirable way. Stratified flows are more frequent with high viscosity fluids or high viscosity ratios between fluids [29, 33]. The fluid viscosity can be altered by adding components to make it more viscous such as polymers, or by changing temperature [9].

Third, the most widely used method to control multiphase flows is by tuning fluid velocity. Pumping methods used in microfluidics can easily modulate flow rate that control fluid behavior and droplets sizes [10, 26]. By increasing the flow rates, the flow pattern will become stratified due to prevalence of viscous forces [18, 29, 30, 32]. In addition, when velocity difference increases, the shear forces to normal forces ratio increases and segmented flow turns into stratified flow [29, 31].

And finally, the flow behavior can be also influenced by channel geometry. It has been proved that channels with higher aspect ratios enhance droplet formation [31]. There is no report of the influence of the channel length. The entrance configuration is also another parameter to take into consideration to enhance one behavior or the other and to control droplet size [9, 10, 26, 37].

All these factors give the framework that designers will use to delineate multiphase microfluidic systems. The aims of many researchers are to achieve reproducibility and fully control of microscale multiphase flows to use these systems in multiple applications. Some examples of multiphase applications are: microreactions and

molecular transport (enzyme kinetics, protein crystallization, syntesis of nanoparticles)[8, 35, 36, 38, 39], solvent extraction [18-20, 34], drug encapsulation and mixing [9, 10, 26].

3.2. Convective Transport Enhancements

In microfluidics, one of the major challenges is to achieve rapid and effective mixing. This is because at microscales the flow is laminar and mixing is usually diffusion limited. In addition, the Péclet number, given by $Pe = \frac{LU}{D}$ where L is the channel characteristic length, U fluid velocity and D diffusivity, is usually very high in theses systems which implies long devices and large diffusion times to achieve full mixing.

In the case of two-phase systems, both diffusion within the phase and diffusion across the interface need to be maximized. Here, three different techniques to enhance molecular transport at microfluidic interfaces and inside the phases are presented.

Droplet Enhancement

Rapid mixing can be conducted due to the convective enhancement produced by two recirculating flows inside of the droplet (Fig. 3.1), which mix the molecules within the phase and also increase the diffusion through the interface by enhancing mass transport to the fluid-fluid interface [8, 18]. In addition, droplets enhance partitioning across interfaces due to the total interface surface area is being increased.

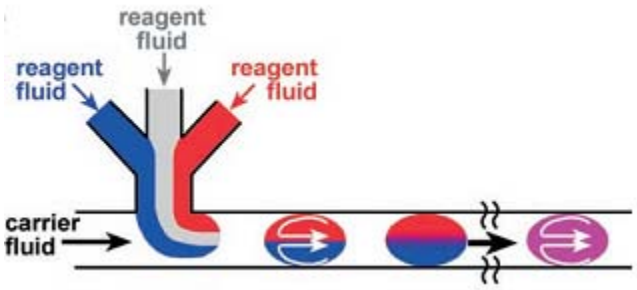

Figure 3.1. Illustration of mixing in a droplet by recirculating flows. Image taken from [8].

Chaotic Advection

Phase mixing can passively enhanced by chaotic advection that occurs in serpentine-liked structures where each direction change will promote the mixing inside of each phase due to the chaotic particle trajectories [8, 40, 41]. Both stratified and droplet-based flows could be benefited by this mixing. In Fig. 3.2, droplet enhancement and chaotic advection mixing strategies are combined showing how recirculating flows are reoriented from the direction of the droplet movement, streached and fold, resulting in a more efficient mixing.

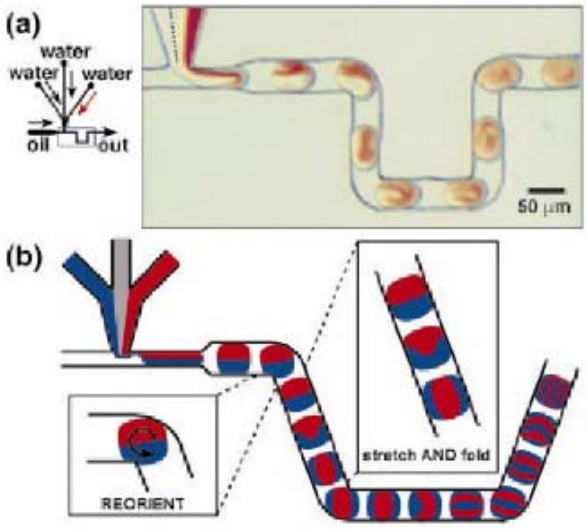

Figure 3.2. Droplets moving through a winding microchannel, a) experimentally and b) schematically. Image taken from [42].

EHD Instability

Electrohydrodynamic instability mixing is an active mixing method which induces an unstable motion at the interface between two solution phases by the application of an external electrical field [4, 20]. Parallel electrodes are located along the microchannel to establish the electrical field. At a critical voltage the interface becomes unstable and the phases start to mix (Fig. 3.3).

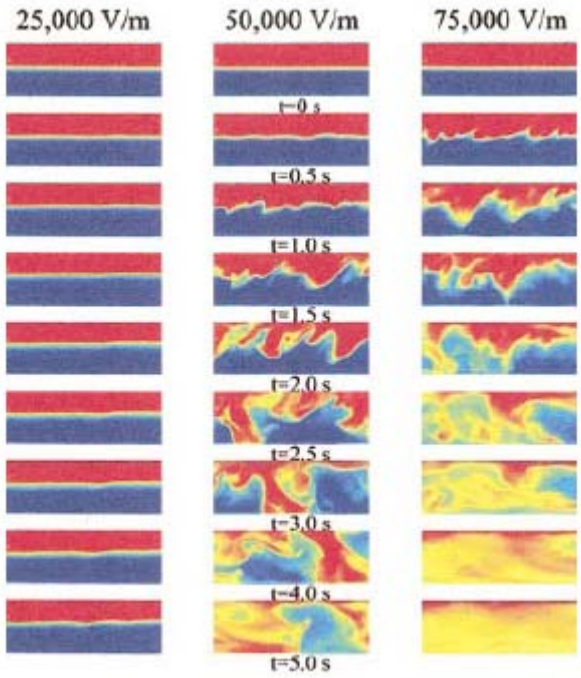

Figure 3.3. Mixing by electrohydrodynamic instability. Image taken from [43].

Droplet enhancement was used in this work to improve transport of proteins to the interface and compared with the partitioning by diffusion in stratified flows. The other transport enhancements will be considered in future works as improvements of this study.

3.3. Separation in Two-Phase Systems: Mechanism of Partitioning

In a two-phase system, partitioning consists of a selective distribution of solute according to their properties [44]. The mechanism of partition is complex and difficult to describe. The solutes are affected by multiple forces including hydrogen bonding, ionic, hydrophobic, van der Waals and other weak forces with the surrounding fluid phase and interactions with other molecules which affect the transport [44]. The contribution of

each force is difficult to calculate; however, the net effect can be characterized by the partition coefficient:

$$K = \frac{C_1}{C_2} \tag{3.6}$$

where C_1 and C_2 are the concentrations of the partitioned molecule at equilibrium in each phase [44]. The partition coefficient is function of the properties of the two phases, molecular characteristics, such as size and charge, and temperature, but ideally independent of concentration [44].

In a two-phase system, the distribution of the molecules is driven by two main phenomena, the thermal motion of the molecules that distributes them in each phase, and the partitioning forces, mentioned previously, which move the solute from one phase to the other. These interactions can be related as:

$$\frac{C_1}{C_2} = e^{-\Delta E / kT} \tag{3.7}$$

where ΔE is the energy required to move a molecule from phase 1 to phase 2, k is the Boltzmann constant, and T is the temperature [44].

In this work the partitioning coefficient for each cell component is fixed because the fluid phase will not be altered from those standardly used in macroscale systems.

This review of the theoretical aspects of multiphase microfluidic system will provide the central guidelines for the design of the DNA purification module addressed in the following chapter.

Chapter 4

Fabrication, Materials and Methods

4.1. Overview

In this chapter the design and fabrication process of the microfluidic device used in this work are discussed, as well as materials and methods utilized in the project. The design of the microchannel involves criteria that satisfy required flow conditions, diffusion time and length, and limit the pressure drop across the device. The channel pattern is then transferred to a mask which is used to create features by photolithography. The microfluidic channels are made of polydimethylsiloxane (PDMS) by casting, or soft lithography, and finally bounded to glass. The aqueous phase and the organic phase are described this section as well. Lastly, the quantification methods used to analyze the efficiency of the design are presented to lead to a better understanding of the results in the following chapter.

4.2. Design of the Serpentine Device

The first goal of the design was to create a microfluidic channel where a stratified flow profile predominates. In that system, the protein partitioning and DNA purification will

occur by only passive diffusion. This represents our control or point of reference to which other types of mixing can be compared.

The first design used a Capillary number criterion and required residence time. As shown in chapter 2, *Ca* is the ratio of viscous and interfacial forces ($Ca = \frac{\mu U}{\gamma}$). It depends directly on the fluid velocity that can be expressed as distance traveled for diffusion within the device over time. Now, let's consider that time as the residence time:

$$t_r = \frac{w^2}{4D} \tag{4.1}$$

where *w* is half the width channel and *D* is the diffusion coefficient of the molecules to be extracted. t_r represents the average time a species must travel to reach the interface. Then, t_r is replaced in $U=L/t$, and plugging *U* in *Ca* equation yields:

$$Ca = \frac{\mu L 4D}{\gamma w^2} \tag{4.2}$$

Ca is now represented in terms of channel length and width. The relationship between channel geometry and *Ca* are shown in Fig. 4.1. Assuming the stratified flow condition and based on previous work with phenol as the organic solvent [19], a minimum *Ca* was used as one of the design criteria, making it equal to 0.3 to guarantee a stratified flow profile. According to this criterion and selecting three different channel widths, 60, 80, and 100 μm, the channel length required in order for all material to be extracted by diffusion should be 11, 20, and 31 cm for each width, respectively. In this calculation, the viscosity used to evaluate the *Ca* was the organic phase's viscosity and the diffusion coefficient utilized was the bovine serum albumin diffusivity which is $6.1*10^{-11}$ m^2/s.

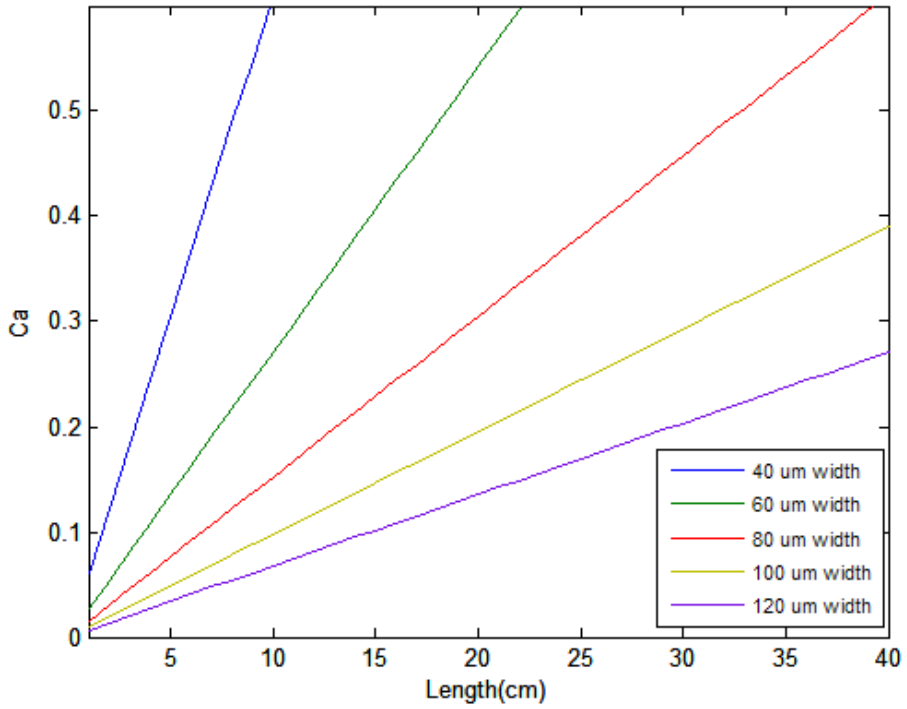

Figure 4.1. Capillary number as a function of geometry characteristic of the channel.

The other design criterion was the analysis of the diffusion problem as 1-dimensional unsteady diffusion, where the gradient in the direction of the channel width is the only one in consideration, which can be written as follows:

$$\frac{\partial C}{\partial t} = D\frac{\partial^2 C}{\partial y^2} \tag{4.3}$$

where C is the concentration of the solute in the aqueous phase and D is the diffusion coefficient. The boundary conditions are no penetration at the channel wall $\frac{\partial C}{\partial y} = 0$, instantaneous partitioning at the surface and so when t goes to infinity C tends to zero at the interface (y=w) and the initial condition is C=Co everywhere at t=0.

By separation of variables, the species concentration profile as a function of space and time can be solved as

$$C = C_o \left[\sum_{i=1,3,5\ldots}^{\infty} \frac{4}{i\pi} \sin\left(\frac{i\pi y}{4a}\right) Exp\left(-\frac{(i\pi)^2 Dt}{16a^2}\right) \right] \tag{4.4}$$

where a is a half of the aqueous phase width. Using the same widths for the previous criterion, 60, 80, and 100 μm, the relative concentrations at different times can be plotted as function of the aqueous phase's width, which is half of the microfluidic channel width, as it shown in Fig. 4.2.

For each channel's width, the time required to reach 1% of C_o was used to calculated the channel's length, assuming velocity U= 0.85 cm/s (Ca~0.3). The required lengths were in 34, 46, 64 cm for widths of 60, 80, and 100 μm, respectively.

The final consideration was the pressure drop in the device. As the length of the device increases, more pressure is required to move the fluid inside of the microchannel. In the device design, the pressure drop was limited by the tubing sealing (J-B kwik) and by the PMDS-glass bond. The pressure drop can be approximated by:

$$\Delta P = \frac{12 Q \mu L}{w h^3} \tag{4.5}$$

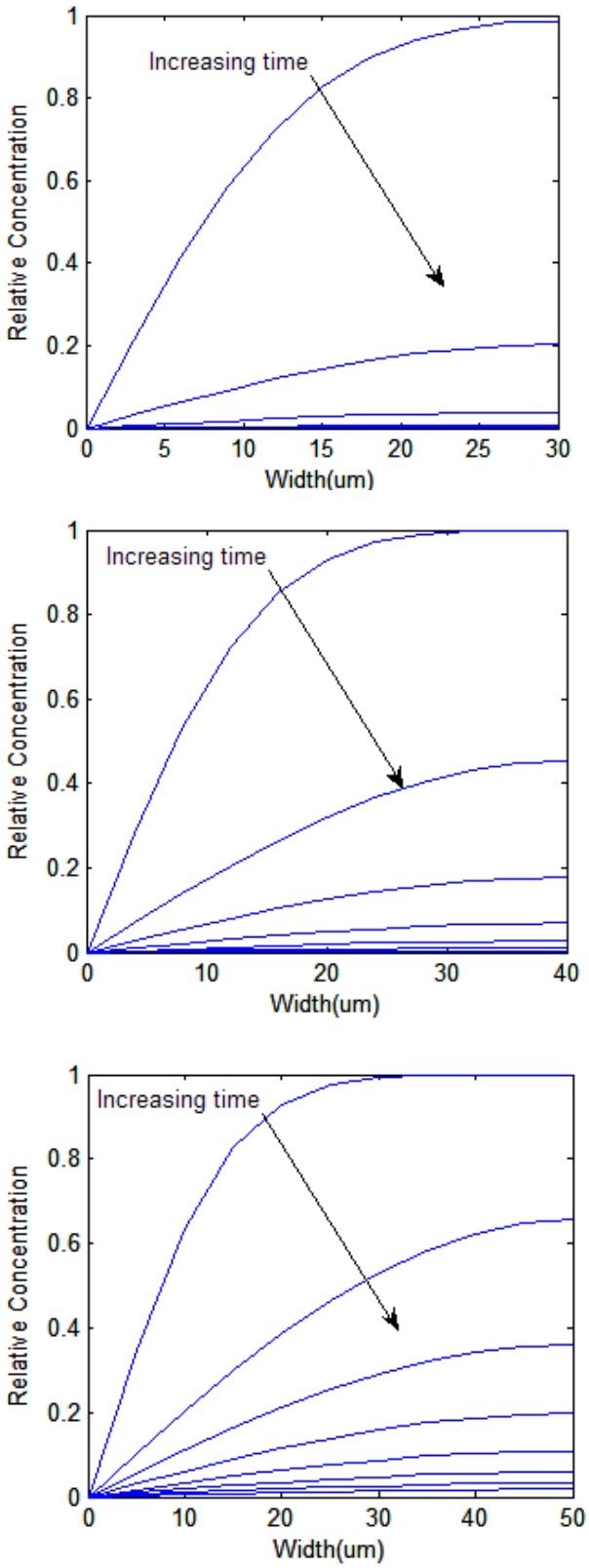

Figure 4.2. Relative concentrations across the channel at different times for each design.

The final dimensions were enlarged to 42 and 57 cm for 60 and 80 μm wide channels, but maintaining 64 cm for the 100 μm wide one for problems of space in the mask. In all cases, the pressure drop was below 2 Atms for the lower thickness (20 μm) that is safe for the sealing and the bonding. Reservoirs, added to insert tubes at inlets and outlets, are designed with a round shape, instead of square, to diminish the presence of air bubbles at the corners. In Fig. 4.3 the final design is shown as appears in the photolithography mask.

4.3. Microchannel Fabrication

The fabrication process of the device involves two different techniques, photolithography and soft lithography. Photolithography is used to transfer a negative pattern from a mask onto a glass slide or silicon wafer, which is called master [45]. Soft lithography is basically a microcasting of the master using an elastomeric material, hence the use of the term *soft* [46].

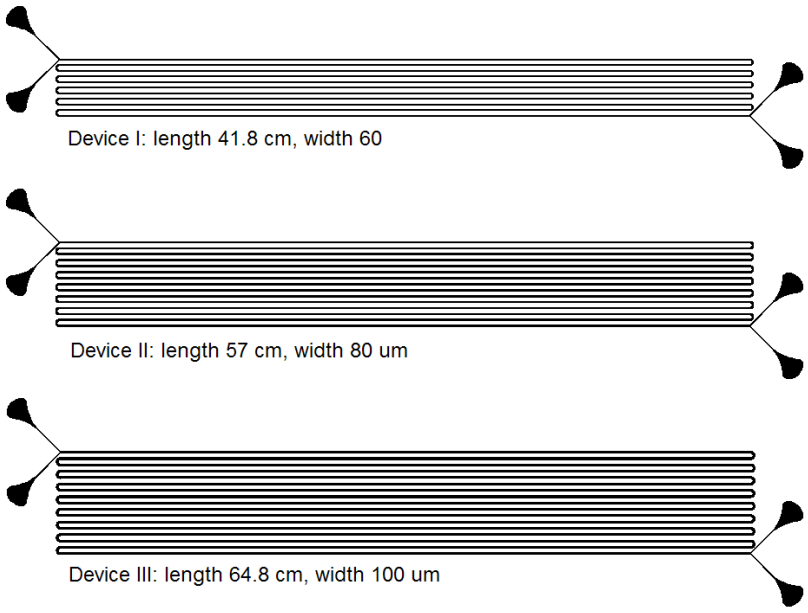

Figure 4.3. Final designs of the serpentine device.

The fabrication is described here but specific process steps are detailed in the Appendix.

First, the microchannel designed in the previous section is transferred to a photolithography mask, which is a glass or quartz plate with patterned metal on it. The master is based on a substrate that is physically and chemically modified to create the patterns on it. Silicon wafers or glass slides are typically used as substrate for the master. Second, the substrate is cleaned and dehydrated at 150 ˚C for 30 min. Third, it is spin coated with negative photoresist SU-8 (MicroChem, Newton, MA) and baked on a hot plate to remove solvents (soft bake). Fourth, the substrate is aligned with the mask in a contact printer and exposed to UV light. The incident light initiates the photo-cross-linking process rendering the exposed parts insoluble. After exposure, the substrate is baked again to remove residual solvent and to densify the film (post exposure bake). Finally, the substrate is immersed in the developer to remove the unexposed photoresist. With these steps, the master mold is ready.

To make the PDMS channels, the elastomer base and elastomer curing agent (Sylgard 184 Silicone Elastomer Kit, Dow Corning, Midland, MI) are mixed at a ratio of 10:1 and poured on top of the master. After getting rid of all air bubbles by using a vacuum chamber, the PDMS mold is cured in an oven at 65 ˚C for 2 hours. When it is solid, the PDMS structure is peeled off the master containing the microchannel and the master is ready for molding more replicas.

A schematic of photolithography and soft lithography process is shown in Fig. 4.4.

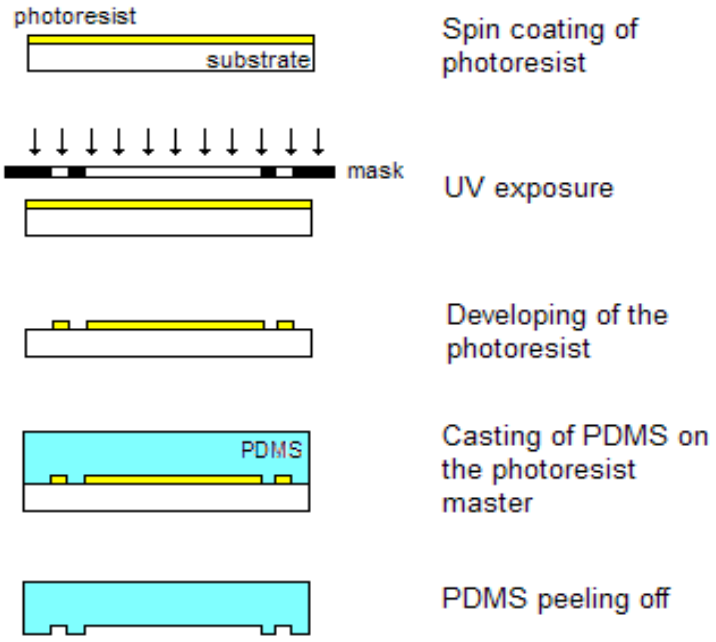

Figure 4.4. Photolithography and soft lithography processes.

Next, the reservoir areas are punched off to allow the entrance and exit of the fluids. The PDMS structure is then bounded to a glass slide by using a corona discharge generator that modifies both the PDMS and glass surfaces enhancing the bonding.

Finally, the device is connected with Tygon tubes (Small Parts Inc., Miami Lakes, FL) and sealed with glue (JB-kwik), specially selected due to their compatibility with the organic phase.

4.4. Aqueous Phase

The aqueous phase basically consists of a buffer solution that contains our biological components of interest, proteins and DNA. The buffer chosen was phosphate buffered saline (PBS) from Hyclone, Thermo Scientific, Longan, UT. To reduce the surface

tension and achieve interfacial stabilization when this phase is in contact with the organic phase [19], sodium dodecyl sulfate (SDS), from J. T. Baker Chemical Co., Phillipsburg, N J, was incorporated at a concentration of 0.5%. SDS is an amphipathic molecule, which means that it has both hydrophobic and hydrophilic regions, where the polar head stays in the aqueous phase and the hydrophobic tail in the organic phase. This amphipathic characteristic makes it possible to reduce the interfacial tension between both phases [19].

The analytes introduced in the aqueous phase are bovine serum albumin protein (BSA) (Omnipur, fraction V; EMD Biosciences) conjugated with rhodamine fluorescent dye and 2-log DNA ladder (0.1 to 10.0 kb; New England Biolabs, Beverly, MA) labeled with YOYO-1 fluorescent dye (Molecular Probes, Invitrogen). The protein concentration selected was 0.3 μg/μl which had enough fluorescence signal to be captured by the camera and while not causing precipitation of proteins or clogging in the microchannel due to high concentrations. Labeling protocols are explained in Appendix.

4.5. Organic Phase

The organic phase is made of a mixture of three components: phenol, the main solvent, chloroform, and isoamyl alcohol, at 50, 48 and 2% volume concentration, respectively. The mixture was purchased from Pierce (Rockford, IL) and used as received.

The main physical properties of the aqueous and organic phase are given in Table 1.

Table 1. Physical properties of the fluids used.

Solution	Density (kg/m^3)	Interfacial Tension (mN/m)	Dynamic Viscosity at 25˚C (Pa.s)
Organic	1330	-	0.00352
Aqueous	1000	-	0.001
Interface	-	0.1	-

4.6. Measurement Methods

As was mentioned in the introduction, protein partitioning and DNA purification are the main purposes of the device of study. To quantify protein depletion, epifluorescence microscopy and spectrophotometry were used. On the other hand, DNA extraction was characterized by spectrophotometry and gel electrophoresis analysis.

The use of fluorescence dyes and particles has been increased in the past decades, being a tremendous instrument to understand cell and molecular biology [47]. Fluorescence is basically the emission of lower energy photons due to the absorption of higher energy incident light or excitation. The emission wavelength is always longer than the excitation wavelength due to energy loss from excitation to emission. The principle of the fluorescence microscopy is based on that difference in excitation and emission wavelengths. By the use of appropriate filters, the exciting light can be completely filtered out without blocking the emitting light, and only the fluorescent object can be seen. The light intensity can be recorded and processed by using digital cameras to track, to quantify, to identify pathways, etc.

To analyze the fluorescence intensity in the channel, a Nikon Eclipse TE2000U inverted epifluorescence microscope (Nikon, Tokyo, Japan), Nikon arc lamp and charged coupled

device (CCD) camera (PowerView 1.4 MP, TSI) were used to capture the images. The relative intensity at different positions in the serpentine device is a useful tool to track the protein partitioning from one phase to the other. The image processing was done by using ImageJ software (NIH Image).

The second method, spectrophotometry, is a well-used technique for quantification of a solute's concentration based on their absorption or transmission properties. In a spectrophotometer, a cuvette that contains the sample is exposed to stream of photons. Some of them will be absorbed by the analytes in the sample solution and the rest will be detected by a light sensor. The logarithm of the ratio of detected light to the incident light is called the absorbance *A*. The absorbance spectrum shows how the light absorbance depends upon the wavelength of the incident light. For a specific analyte, the concentration could be calculated by analyzing the absorbance spectrum due to its proportionality to the amount of analyte in the sample.

Finally, agarose gel electrophoresis analysis was used to quantify DNA fragments at the entrance and the outputs of the device. With this technique, DNA fragments can be separated, identified and purified based on their size. DNA samples are loaded into an agarose gel with a low concentration of the fluorescent dye ethidium bromide which intercalates with DNA and makes it easy to detect under ultraviolet light. The gel with the samples is submerged in a buffer-filled chamber, which contain electrodes, locating the samples wells at the negative electrode side. When a voltage is applied, DNA fragments migrate towards the positive electrode side as they are negative charged. Fragments travel with mobility inversely proportional to their size. In other words, smaller fragments can travel faster in the gel or matrix than large fragments of DNA. Based on this

characteristic, DNA size and concentration can be identified and quantified using image processing of the gel.

In the following chapter, the experimental results will show device performance using the materials and methods described here.

Chapter 5

Results and Discussion

5.1. Experimental Setup

Devices were fabricated as described in the previous chapter. In Fig. 5.1, a photograph of the device shows the microchannel platform where the DNA extraction was performed. Inlet and outlets were unglued for the photograph to show the reservoirs and food coloring was used to highlight the channels.

The experimental setup consisted of the device, two glass syringes (Hamilton, Reno, NV) for infusion of the aqueous and organic phase, syringe pumps to control flow rates (Harvard apparatus, Holliston, MA), and Eppendorf tubes to collect the output.

The filling procedure was the most critical part of the experiment. This step was crucial to get rid of air bubbles inside of the microchannels, to avoid pressure differences between inlets and to prepare and wet the device's wall. The first step of the procedure was to fill the device with a PBS solution containing 0.5% SDS at the aqueous inlet and leaving the other three tubings open to allow the air to escape. When the whole device was filled with the aqueous solution, the organic phase was introduced, and flow rates of both inlets were established to achieve parallel flows through the serpentine device. After

maintaining the parallel flow for a few minutes, the PBS solution was switched to the aqueous phase containing the analytes.

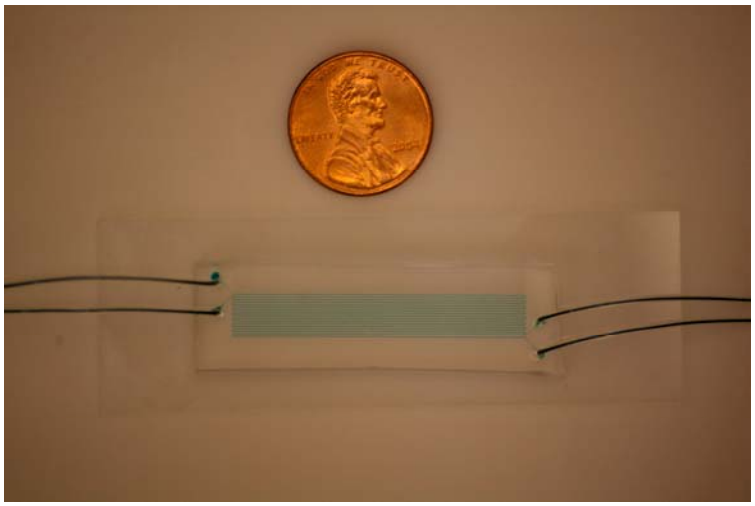

Figure 5.1. Photograph of the serpentine device.

A first attempt using a device with a 50 μm channel height was not successful due to problems establishing the parallel flow through the serpentine device. The aqueous phase was frequently located in the middle of the device, avoiding the hydrophobic walls, and having a sandwich-like aspect (organic-aqueous-organic). This situation greatly improved after reducing the height of the channel to 20 μm. This allowed enclosing the phases and forcing them to stay parallel. After this modification, sandwich-like behavior was less frequent, or it was formed for short periods until the aqueous phase displaced the phenol layer near the wall.

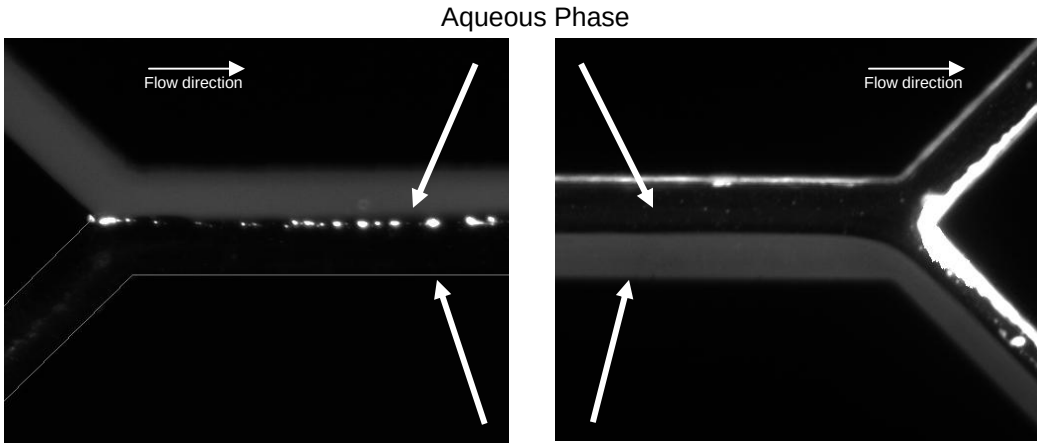

Figure 5.2. Images of the two phases at the entrance (left) and at the outlet (right) of the device II. Rhodamine fluorescent dye labeled BSA is infused at the entrance and removed into the phenol phase at the outlet.

The introduction of rhodamine labeled BSA in the channel led to clogging and precipitation. The initial BSA concentration used was 0. 5μg/μl. At this concentration, precipitation of proteins occurred within the first serpentine's line. Protein began to accumulate at the interface at the entrance of the device (as shown in Fig. 5.2. a). At downstream positions, some of the proteins diffused into the organic phase but others remained in the aqueous phase precipitating or adhered on the walls as it is shown in Fig. 5.3. In addition, high concentrations of proteins caused clogging of the outlets in the shortest device. These problems were partially solved by reducing the BSA concentration to 0.3 μg/μl without dramatically affecting the image analysis. Small precipitation and accumulation on the wall were still observed at the first 3 centimeters but in lower proportions.

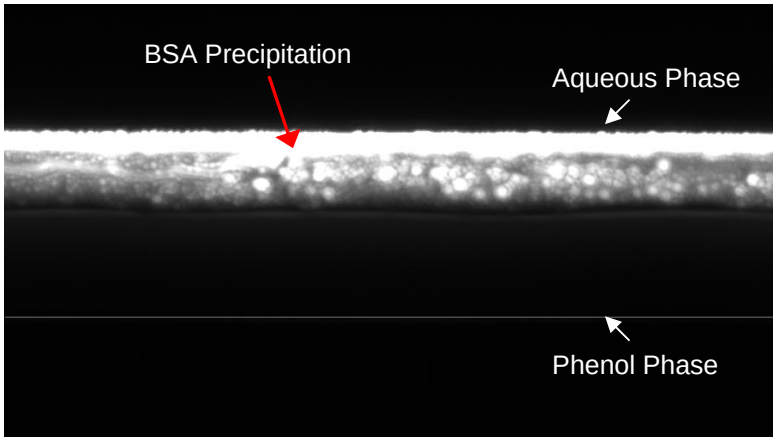

Figure 5.3. Image of BSA precipitation in the aqueous phase at 0.50 µg/µl concentration.

5.2. Comparison of BSA depletion between the three devices.

The designs presented in the previous chapter are compared here. The devices were compared based on their BSA depletion efficiency. The experimental conditions are explained below.

The first experiments were realized using the largest device (device III). For this particular geometry, the parallel flow was achieved in the entire serpentine structure only at high flow rates, 3 µl/min for the aqueous phase and 1.3 µl/min for the phenol phase. The mean velocity of the aqueous phase was 5 cm/s, much higher than the velocity used for the design criterion. Reduction of the flow rate involved the generation of droplets at the entrance or in other sections of the device.

The comparison was done using the same mean velocity (5 cm/s) in the aqueous phases of the three different devices. The aqueous flow rates were 2.4 µl/min and 1.8 µl/min for device II and I, respectively. The flow rates for the phenol phase were 1 µl/min and 1.3 µl/min for the same devices.

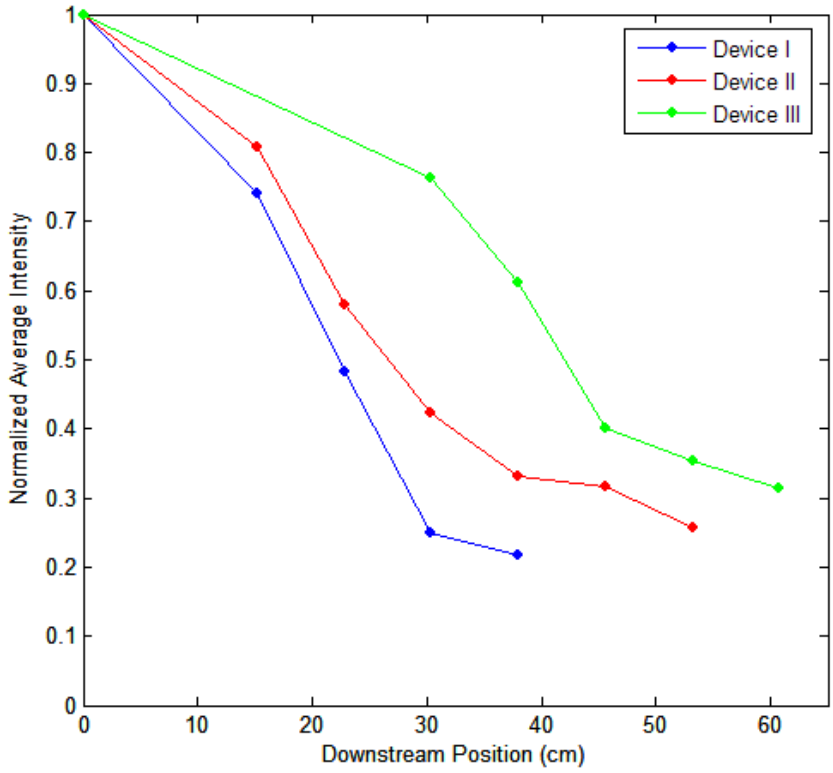

Figure 5.4. Depletion of BSA at different downstream positions in the aqueous phase of each device.

In addition to the velocity condition, the BSA concentration at the inlet was fixed to 0.3 µg/µl based on the results explained in the previous section. Moreover, the image settings were also fixed for the three devices to 26 ms for the exposure time, using a 10X lens and neutral density filter ND1 for the epiflourescent arc lamp.

During the experiment, images of the phases were taken at different positions along each device. The images were then analyzed, obtaining the average intensity of the aqueous phase at different downstream position and normalized with the average intensity at the inlet. In Fig. 5.4 the depletion of BSA in each device is plotted as a function of downstream position. As was expected, in the narrow channel (device I) the depletion is faster than in wider ones (device II and III). The partition's efficiencies using fluorescence intensity method were 78 %, 74.3 % and 68.5 % for device I, II and III, respectively.

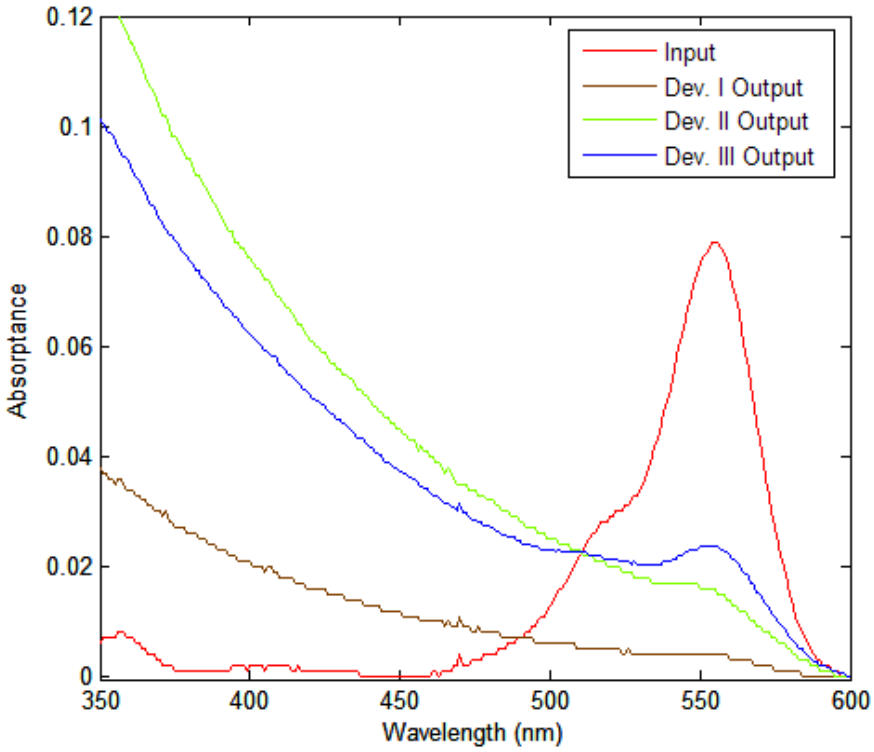

Figure 5.5. Absorption spectra of samples of the aqueous phase inlet and aqueous phase outlets of each device.

During these experiments with rhodamine fluorescent dye labeled BSA, the aqueous phase outputs were collected and analysed by spectrophotometry. The results are shown

in Fig. 5.5. From the spectra, the high absorption at low wavelength was due to phenol contamination found in all the aqueous outputs which could be due to small micelles formed at the interface. According to the ratio of absorption at 555 nm between the inlet sample and the outputs from the different devices, the partitioning's efficiencies were 90%, 78 % and 69 % for device I, II and III, respectively.

From the above comparison, device I seems to be the most efficient one; however, for the following experiments, device II was chosen over device I to avoid future problems of obstruction by lysed cells due to narrow inlets in device I.

5.3. Stratified Flow

In this section, the study of the analytes in the two-phase system under stratified flow condition using only device II is presented. Initially, the experiment was done incorporating only BSA in the aqueous phase, as in the previous section. Then, another experiment was done with only DNA in the aqueous phase. Finally, both BSA and DNA were mixed and introduced in the aqueous phase to analyze partitioning and purification at the same time.

The experiment with only BSA using device II was presented above in this chapter. Here, channel cross section fluorescence profiles at the inlet and outlet can provide an alternative approach to demonstrate the partitioning of rhodamine conjugated BSA from the aqueous phase to the organic phase (Fig. 5.6). Absorption spectra are shown in Fig. 5.7.

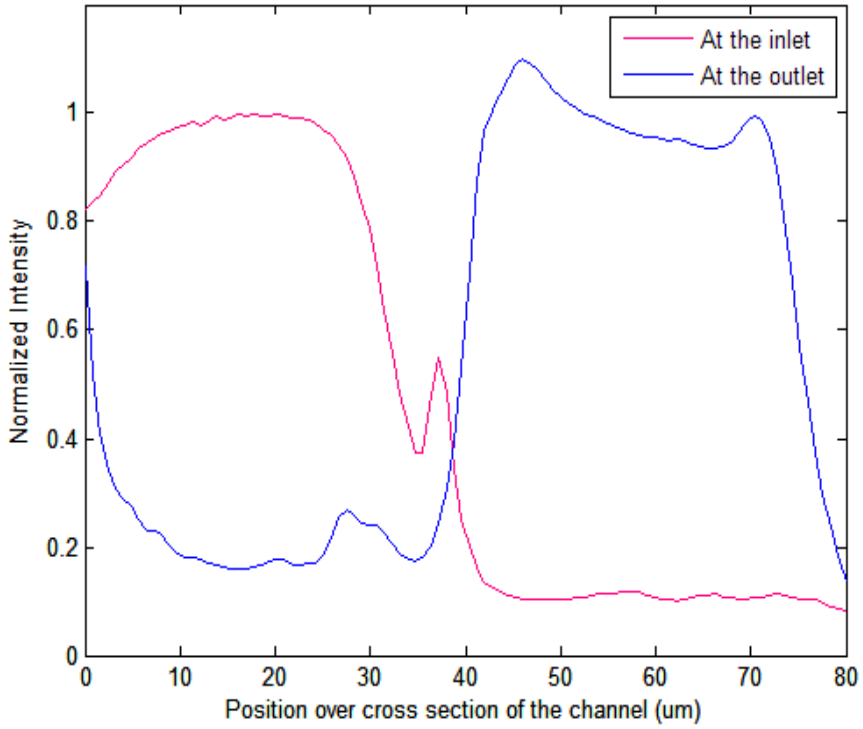

Figure 5.6. Normalized intensity profiles of rhodamine conjugated BSA at inlet and outlet of the device II.

The second experiment was realized using only DNA in aqueous phase. The results obtained by spectrophotometry show a high recovery at the aqueous outlet as was expected (Fig. 5.8). Gel electrophoresis analysis of inlet and outlet samples in Fig. 5.9, using ImageJ to quantify the total intensity in each lane, resulted in 99% recovery of DNA.

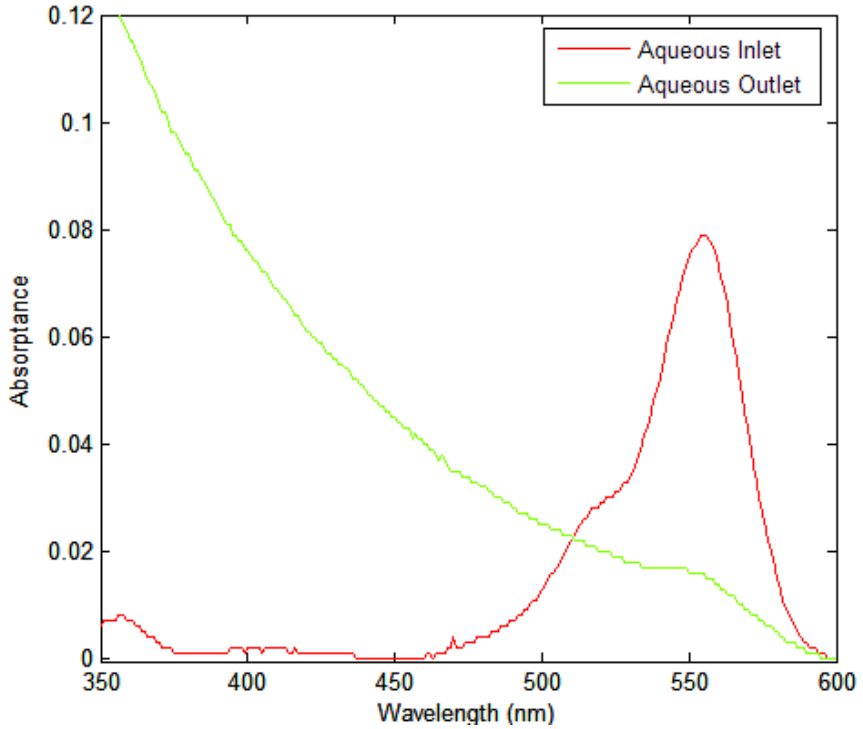

Figure 5.7. Absorption spectra of the aqueous phase inlet and outlet. Only rhodamine conjugated BSA is present in the aqueous phase inlet.

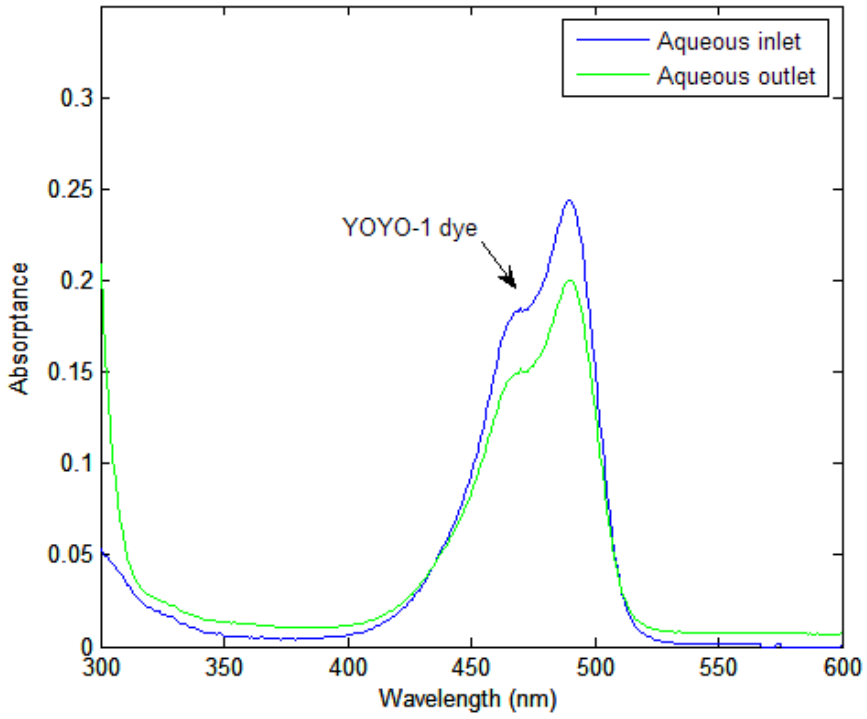

Figure 5.8. Absorption spectra of the aqueous phase inlet and outlet. Only YOYO-1 labeled DNA is present in the aqueous phase inlet.

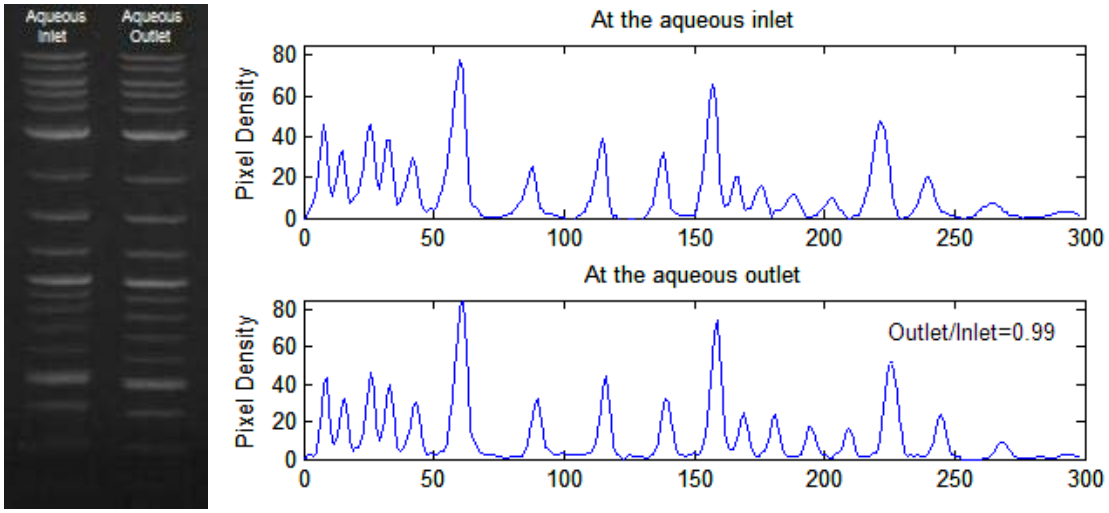

a) b)

Figure 5.9. Incorporation of only DNA in the aqueous phase: a) Agarose gel electrophoresis analysis of inlet and outlet samples, b) Pixel intensity analysis of the gel lanes.

The next step was to mix BSA and DNA together in the aqueous phase. Absorption spectra analysis and gel electrophoresis analysis were conducted (Fig 5.10 and Fig. 5.11, respectively).

When both DNA and BSA are present, the absorption spectra (Fig. 5.10) show partitioning of BSA to the organic phase, similar to the experiments without DNA (Fig. 5.7). However, in Fig. 5.10, high absorption at the YOYO-1 dye wavelength is present in the organic outlet instead of the aqueous phase where DNA is expected to be, based in the experiment without BSA (Fig. 5.8). Nevertheless, gel electrophoresis results in Fig. 5.11 determined that DNA is present in the aqueous outlet, and not in the organic outlet, leading to the hypothesis that YOYO-1 dye intercalation could be affected by the presence of organic solvents and could be partitioning to the organic phase.

Gel electrophoresis analysis results show that, in proportion, the aqueous outlet intensity is larger that the aqueous inlet intensity with outlet-to-inlet ratio of 1.07 (Fig. 5.11b). The higher DNA concentration at the aqueous outlet could be either due to evaporation during the collection of the sample, uneven loading of the gel, or to a concentrating effect due to the presence of the organic phase. Nevertheless, only a very small amount of DNA was found in the organic outlet (9 %); consequently, the purification efficiency using stratified flows was approximately 90%.

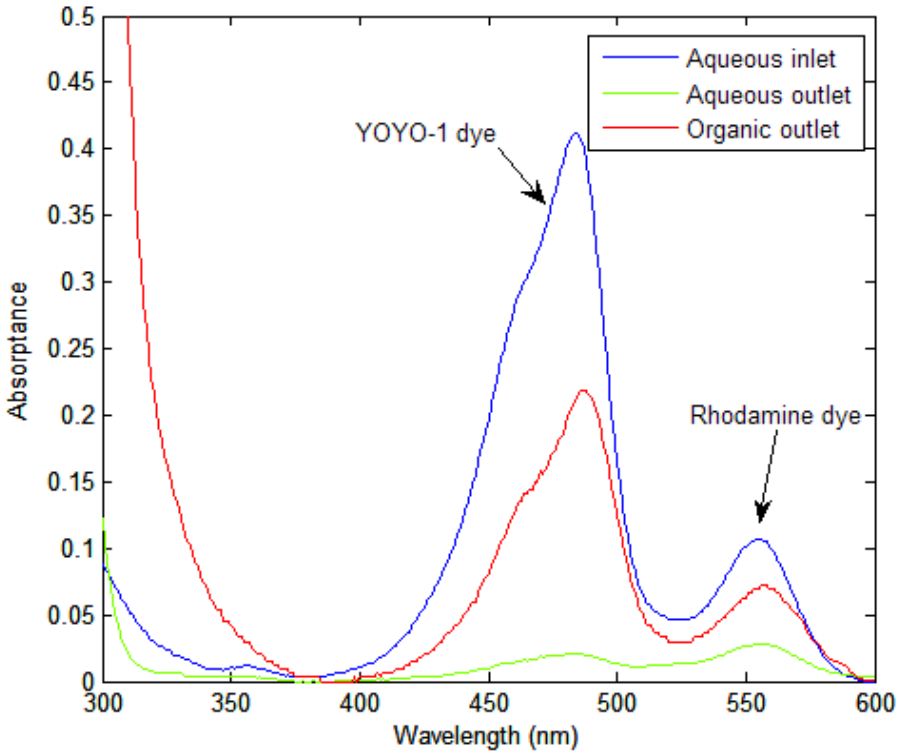

Figure 5.10. Absorption spectra of the aqueous phase inlet and outlet. Both rhodamine conjugated BSA and YOYO-1 labeled DNA are present in the aqueous phase inlet.

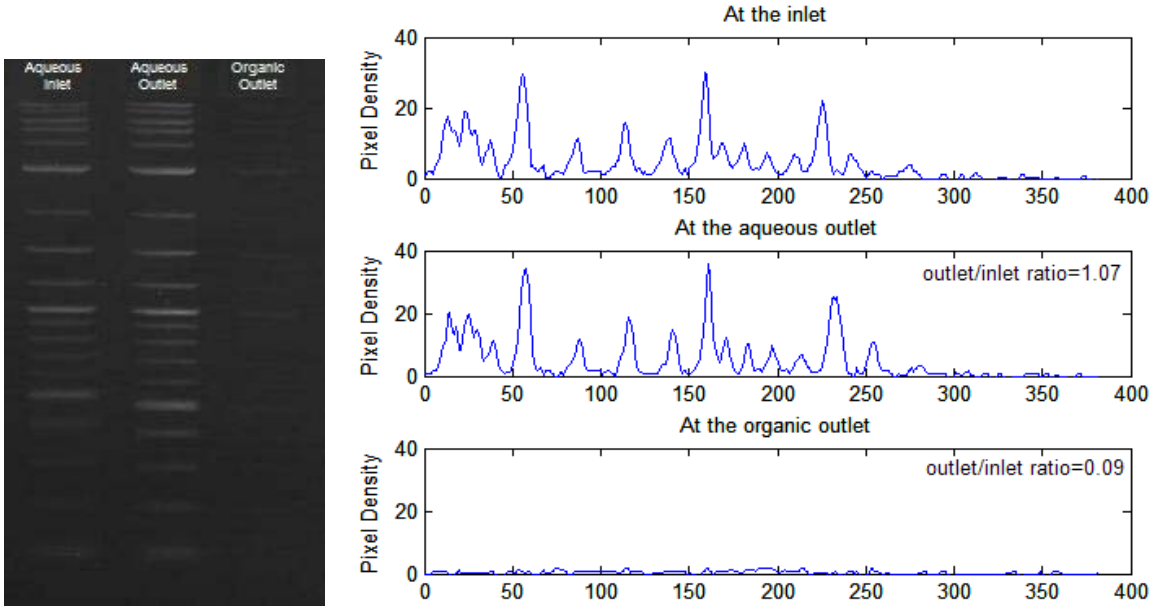

a) b)

Figure 5.11. Incorporation of DNA and BSA in the aqueous phase: a) Agarose gel electrophoresis analysis of inlet and outlet samples, b) Pixel intensity analysis of the gel lanes.

5.4. Droplet Formation

Protein partitioning and DNA purification was also analyzed using droplet-based flows. In this experiment, the serpentine device II was used, like in the previous experiment, but the channel height was increased to 50 µm to improve droplet formation.

The flow rates used were 0.5 µl/min for the phenol phase and 0.35 µl/min for the aqueous phase. In this case, droplet formation was easy to obtain by making the flow rate of the phenol phase (the most viscous phase) faster than that of the aqueous phase. This flow rate ratio agrees with two-flow pattern diagrams produced by others researchers where droplet formation occurred at low flow rates with oil phase flow rate larger than the aqueous phase flow rate [31].

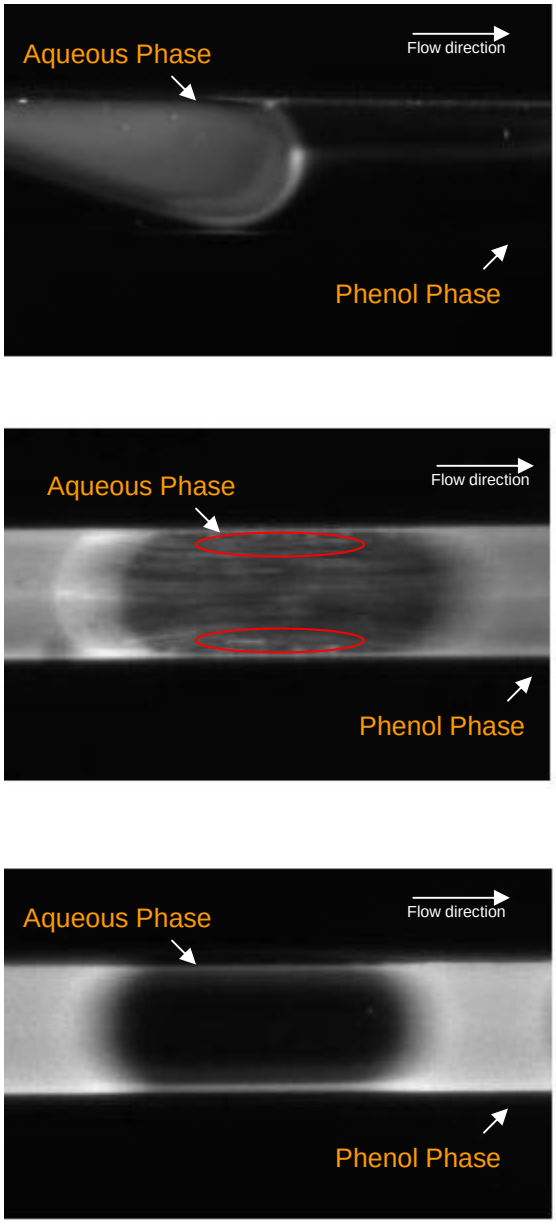

Figure 5.12. Images of three different downstream position using rhodamine conjugated BSA (top: at the entrance, middle: at 3 cm of the entrance, bottom: at the outlet).

In the aqueous inlet both rhodamine conjugated BSA and YOYO-1 labeled DNA were introduced and droplet formation was obtained with phenol as the carrier fluid. The output of this experiment was a mixture of the two phases which were phase separated by density and micropipette tools outside of the device.

In Fig 5.12 images at different positions in the device demonstrated the effective depletion of BSA with this mixing method. In the same figure, the image at the middle shows the formation of two recirculating flows inside the droplet which enhances the mixing and convective transport of BSA to the interface for more effective partitioning.

Protein partitioning was more effective using droplet formation enhancement as it can be observed in the images (Fig. 5.12) and in the intensity profiles (Fig. 5.13). Using fluorescence intensity analysis from images at the inlet and outlet, the partitioning efficiency using droplets was 88 %.

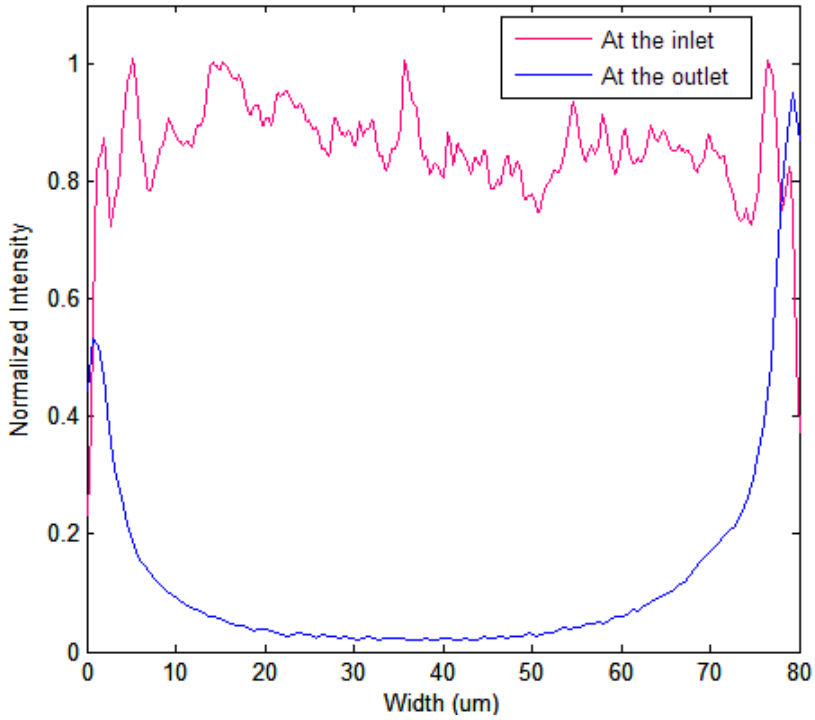

Figure 5.13. Normalized intensity profiles of rhodamine conjugated BSA at inlet and outlet of the device II using droplet-based flow.

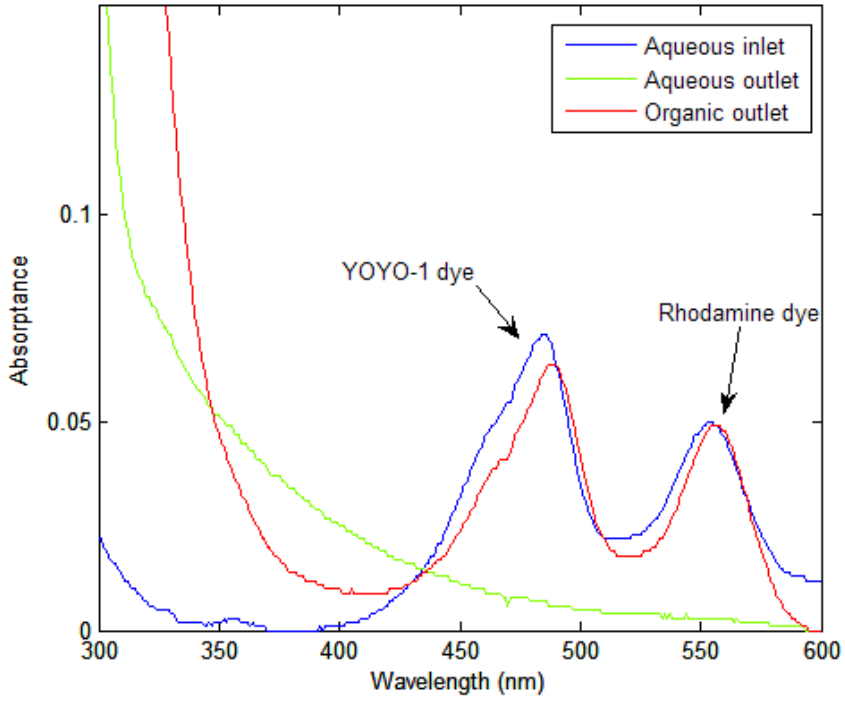

Figure 5.14. Absorption spectra of the aqueous phase inlet and outlet for droplet-based experiment. Both rhodamine conjugated BSA and YOYO-1 labeled DNA are present in the aqueous phase inlet.

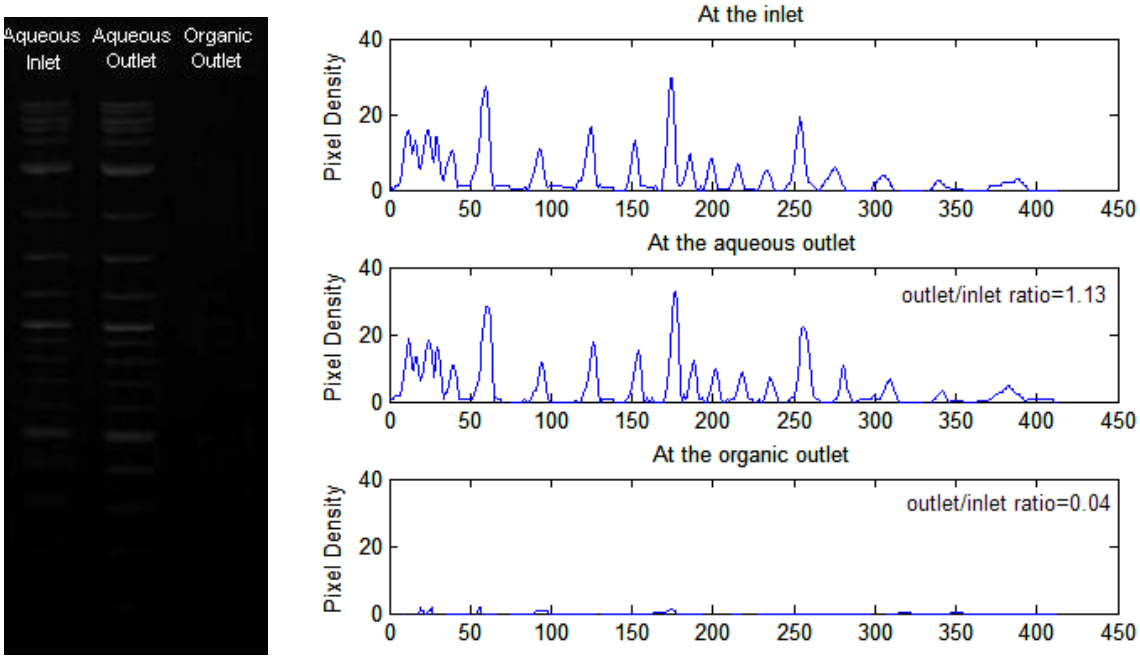

a) b)

Figure 5.15. Droplet-based experiment. a) Agarose gel electrophoresis analysis of inlet and outlet samples, b) Pixel intensity analysis of the gel lanes.

From the spectrophotometry result shown in Fig. 5.14, it seems that the partitioning was more efficient in this case of droplet-based flow if it is compared with the same results found for stratified flow in Fig. 5.10. In addition, the concentration of YOYO-1 dye in the organic phase was found higher for the droplet-based experiment. Consequently, the hypothesis of partitioning of the DNA dye to the organic phase takes more significance. As a result of the convective enhancement, the dye depletion was also increased in droplet-based flows.

Nevertheless, DNA stayed in the aqueous phase as shown by the gel electrophoresis analysis (Fig. 5.15), similar to the previous experiment using stratified flow. If the concentration of DNA in the organic phase is compared, a smaller amount of DNA was found in the organic phase during droplet formation and the purification efficiency was

approximately 96%. Therefore, droplets could also enhance the compartmentalization of DNA, in addition to the protein partitioning improvement.

In summary, experimental results showing DNA extraction with two-phase flows were presented and discussed in this chapter. The experiments were conducted in different devices to compare them based on protein partitioning. In addition, partitioning and DNA purification were analysed under both parallel-flow and droplet-formation conditions.

Chapter 6

Conclusions and Future Work

In this thesis partitioning of proteins and DNA isolation were evaluated in long microfluidic devices under stratified and droplet-formation flow conditions. From the experiments, protein precipitation and clogging problems forced the use of dilute samples and to avoid narrow channels. Furthermore, phenol contamination was found in the aqueous phase, which could be due to the formation of micelles at the interface and will need to be solved, for instance, with a further decontamination step.

The two-phase system was analyzed under two different flow patterns (stratified and droplets-based) to investigate the mixing of the phases and the solutes. The experimental results show that the droplet formation seems to enhance both protein partitioning and DNA purification efficiencies.

In both flow patterns, YOYO-1 dye seems to partition to the phenol phase according to the spectrophotometry results. In addition, a possible problem of evaporation found in both experiments during the sample collection could be the reason of higher DNA concentration at the aqueous outlet in the agarose gel. Future experiments will require sealing the sample container during the recollection.

In stratified flows, partitioning can be improved adding other extraction station steps in a serial manner. The serpentine design could be divided into two stations and will require one output removing the phenol with proteins, and another input adding clean phenol. This new station can improve efficiency and probably reduce time if the diffusion length required is smaller than in the previous design.

In droplet-formation flows, a new device needs to be designed because the device used was planned for stratified flows. Using droplet enhancement the length of the device can be much shorter. It could be redesigned to enhance the formation of droplets, for example, by using T configuration at the fluid entrance. Computational Fluid Dynamic (CFD) softwares could help to simulate different flow conditions and to identify an optimal design. In addition, droplet-based flow will require a manner to separate the phases into parallel flows inside the device and to permit the recollection of each phase separately.

Further future directions will include the use CFD programs to analyze two-phase systems, to predict the fluid behavior and to obtain suitable geometry and flow conditions. Computational analysis could be also used to simulate the particle partitioning in parallel flows and to predict the efficiency as a function of the channel geometry and the fluid conditions.

Precipitation with ethanol and resuspention in TE buffer steps will be considered which could be included in a staged device to remove the phenol contamination from the DNA sample. For DNA visualization, covalent dyes, instead of intercalating ones, could be used to prevent their partitioning into the organic phase.

Additionally, the use of transformed bacterial cells to characterize DNA extraction will be part of the future work as well as a comparison of the microfluidic platform with available commercial DNA kits.

Finally, EHD instability and chaotic advection will be considered to improve the mixing and the purification efficiency obtained in the present work.

Bibliography

1. Sambrook, J., E.F. Fritsch, and T. Maniatis, *Molecular Cloning: A Laboratory Manual*. 1989, NY: Cold Spring Harbor Laboratory Press.
2. Qiagen, *QIAprep Miniprep Handbook*. 2003: Qiagen Distributors
3. Nguyen, N.T. and S.T. Wereley, *Fundamentals And Applications of Microfluidics* Second ed. 2006: Artech House Publishers.
4. Berthier, J. and P. Silberzan, *Microfluidics for biotechnology* 2006, Boston, MA: Artech House.
5. Erickson, D. and D. Li, *Integrated microfluidic devices.* Analytica Chimica Acta, 2004. **507**(1): p. 11-26.
6. Squires, T.M. and S.R. Quake, *Microfluidics: Fluid physics at the nanoliter scale.* Reviews of Modern Physics, 2005. **77**(3): p. 977-50.
7. Atencia, J. and D.J. Beebe, *Controlled microfluidic interfaces.* Nature, 2005. **437**(7059): p. 648-655.
8. Helen Song, D.L.C., Rustem F. Ismagilov,, *Reactions in Droplets in Microfluidic Channels.* Angewandte Chemie International Edition, 2006. **45**(44): p. 7336-7356.
9. Shui, L., J.C.T. Eijkel, and A. van den Berg, *Multiphase flow in microfluidic systems - Control and applications of droplets and interfaces.* Advances in Colloid and Interface Science, 2007. **133**(1): p. 35-49.
10. Shui, L., et al., *Multiphase flow in lab on chip devices: A real tool for the future?* Lab on a Chip, 2008. **8**(7): p. 1010-1014.
11. Breadmore, M.C., et al., *Microchip-Based Purification of DNA from Biological Samples.* Anal. Chem., 2003. **75**(8): p. 1880-1886.
12. Tian, H., A.F.R. Hühmer, and J.P. Landers, *Evaluation of Silica Resins for Direct and Efficient Extraction of DNA from Complex Biological Matrices in a Miniaturized Format.* Analytical Biochemistry, 2000. **283**(2): p. 175-191.
13. Christel, L.A., et al., *Rapid, automated nucleic acid probe assays using silicon microstructures for nucleic acid concentration.* Journal of Biomechanical Engineering 1999. **121**(1): p. 22-7.
14. Hong, J.W., et al., *A nanoliter-scale nucleic acid processor with parallel architecture.* Nature Biotechnology, 2004. **22**(4): p. 435-9.
15. Xing Chen, D.F.C., Chang Chun Liu,, *On-line cell lysis and DNA extraction on a microfluidic biochip fabricated by microelectromechanical system technology.* ELECTROPHORESIS, 2008. **29**(9): p. 1844-1851.

16. Joon-Ho, K., et al. *A disposable DNA sample preparation microfluidic chip for nucleic acid probe assay*. in *Micro Electro Mechanical Systems, 2002. The Fifteenth IEEE International Conference on*. 2002.
17. Bhattacharyya, A. and C.M. Klapperich, *Microfluidics-based extraction of viral RNA from infected mammalian cells for disposable molecular diagnostics*. Sensors and Actuators B: Chemical, 2008. **129**(2): p. 693-698.
18. Mao, X., S. Yang, and J. Zahn. *Experimental Demonstration and Numerical Simulation of Organic-Aqueous Liquid Extraction Enhanced by Droplet Formation in a Microfluidic Channel*. in *Proceedings of the ASME IMECE*. 2006. Chicago, IL.
19. Reddy, V. and J.D. Zahn, *Interfacial stabilization of organic-aqueous two-phase microflows for a miniaturized DNA extraction module.* J Colloid Interface Sci, 2005. **286**(1): p. 158-65.
20. Zahn, J. and V. Reddy, *Two phase micromixing and analysis using electrohydrodynamic instabilities.* Microfluidics and Nanofluidics, 2006. **2**(5): p. 399-415.
21. McMillan, W.A., et al. *Application of advanced microfluidics and rapid PCR to analysis of microbial targets*. in *Proceedings of the 8th international symposium on microbial ecology*. 1999.
22. Legendre, L.A., et al., *A Simple, Valveless Microfluidic Sample Preparation Device for Extraction and Amplification of DNA from Nanoliter-Volume Samples.* Anal. Chem., 2006. **78**(5): p. 1444-1451.
23. Wen, J., et al., *Microfluidic-Based DNA Purification in a Two-Stage, Dual-Phase Microchip Containing a Reversed-Phase and a Photopolymerized Monolith.* Anal. Chem., 2007. **79**(16): p. 6135-6142.
24. Easley, C.J., et al., *A fully integrated microfluidic genetic analysis system with sample-in-answer-out capability.* Proceedings of the National Academy of Sciences, 2006. **103**(51): p. 19272-19277.
25. Christopher, G.F. and S.L. Anna, *Microfluidic methods for generating continuous droplet streams.* Journal of Physics D: Applied Physics, 2007. **40**(19): p. R319-R336.
26. Shui, L., J.C.T. Eijkel, and A. van den Berg, *Multiphase flow in micro- and nanochannels.* Sensors and Actuators B: Chemical, 2007. **121**(1): p. 263-276.
27. Purcell, E.M., *Life at low Reynolds number.* American Journal of Physics, 1977. **45**(1): p. 3-11.
28. Brody, J.P., et al., *Biotechnology at low Reynolds numbers.* Biophys. J., 1996. **71**(6): p. 3430-3441.
29. Dreyfus, R., P. Tabeling, and H. Willaime, *Ordered and Disordered Patterns in Two-Phase Flows in Microchannels.* Physical Review Letters, 2003. **90**(14): p. 144505.
30. Xu, J., et al., *Correlations of droplet formation in T-junction microfluidic devices: from squeezing to dripping.* Microfluidics and Nanofluidics.
31. Guillot, P. and A. Colin, *Stability of parallel flows in a microchannel after a T junction.* Physical Review E (Statistical, Nonlinear, and Soft Matter Physics), 2005. **72**(6): p. 066301-4.

32. Tice, J.D., et al., *Formation of Droplets and Mixing in Multiphase Microfluidics at Low Values of the Reynolds and the Capillary Numbers.* Langmuir, 2003. **19**(22): p. 9127-9133.
33. Tice, J., A. Lyon, and R. Ismagilov, *Effects of viscosity on droplet formation and mixing in microfluidic channels.* Analytica Chimica Acta, 2004. **507**: p. 73-77.
34. Hibara, A., et al., *Integrated Multilayer Flow System on a Microchip.* Analytical Sciences, 2001. **17**(1): p. 89-93.
35. Surmeian, M., et al., *Three-Layer Flow Membrane System on a Microchip for Investigation of Molecular Transport.* Anal. Chem., 2002. **74**(9): p. 2014-2020.
36. Tokeshi, M., et al., *Continuous-flow chemical processing on a microchip by combining microunit operations and a multiphase flow network.* Analytical Chemistry, 2002. **74**(7): p. 1565-1571.
37. Link, D.R., et al., *Geometrically Mediated Breakup of Drops in Microfluidic Devices.* Physical Review Letters, 2004. **92**(5): p. 054503.
38. Masumi Yamada, V.K., Megumi Nakashima, Jun'ichi Edahiro, Minoru Seki,, *Continuous cell partitioning using an aqueous two-phase flow system in microfluidic devices.* Biotechnology and Bioengineering, 2004. **88**(4): p. 489-494.
39. Castell, O.K., C.J. Allender, and D.A. Barrow, *Continuous molecular enrichment in microfluidic systems.* Lab on a Chip, 2008. **8**(7): p. 1031-1033.
40. Aref, H., *The development of chaotic advection.* Physics of Fluids, 2002. **14**(4): p. 1315-1325.
41. Liu, R.H., et al., *Passive mixing in a three-dimensional serpentine microchannel.* Microelectromechanical Systems, Journal of, 2000. **9**(2): p. 190-197.
42. Song, H., et al., *Experimental test of scaling of mixing by chaotic advection in droplets moving through microfluidic channels.* Applied Physics Letters, 2003. **83**(22): p. 4664-4666.
43. Lin, H., et al., *Instability of electrokinetic microchannel flows with conductivity gradients*, in *Physics of Fluids*. 2004, American Institute of Physics. p. 1922-1935.
44. Albertsson, P.-A., *Partition of cell particles and macromolecules*. Third ed. 1986, New York, NY: Wiley.
45. Madou, M.J., *Fundamentals of Microfabrication*. Second ed. 2002, Boca Raton: CRC Press.
46. Younan Xia, G.M.W., *Soft Lithography.* Angewandte Chemie International Edition, 1998. **37**(5): p. 550-575.
47. Lichtman, J.W. and J.-A. Conchello, *Fluorescence microscopy.* Nature Methods 2005. **2**: p. 910-019.
48. Shrewsbury, P.J., S.J. Muller, and D. Liepmann, *Effect of Flow on Complex Biological Macromolecules in Microfluidic Devices.* Biomedical Microdevices, 2001. **3**(3): p. 225-238.

Appendix

Photolithography process

Silicon cleaning procedure.

- Dip glass slide in acetone, isopropanol and deionized water baths for 10 minutes each.
- Dehydrated the glass slides at a 150C for 30 minutes in an oven.

Lithography for SU-8 2050 Negative Photoresist

- Dispense the photoresist on the substrate.
- Spin conditions: 30 sec at 1600 rpm.
- Soft-bake photoresist for 2 minutes at 65C and 6 minutes at 95C on a hotplate.
- Expose photoresist under UV light for 20 seconds.
- Post-Exposure bake photoresist for 1 minute at 65C and 4 minutes at 95C on a hotplate.
- Develop photoresist by immersing slide in SU-8 developer for 8 minutes with gentle agitation.
- Gently rinse the slide in D.I water.
- Gently dry the glass slide using an air gun.

BSA Labeling

First, 5-6-carboxy-tetramethylrhodamine (TAMRA) succinimidyl ester dye (Fluka, Switzerland) is dissolved in Dimethyl Sulfoxide (DMSO) (Amresco, Solon, OH) to a concentration of 10 mg/ml. BSA is separately dissolved in PBS to a concentration of 50 mg/ml. Then, the amount of dye to be added to the BSA solution is calculated using the following equation:

$$V_{Rhod}[\mu l] = \frac{C_{BSA} \times V_{BSA}}{MW_{BSA}} \times MW_{Rhod} \times 100 \times MR \quad \text{(A.1)}$$

where C_{BSA} is the concentration of BSA in mg/ml and V_{BSA} is the volume in ml of the BSA solution. MW_{BSA} is the molecular weight of the protein, 66000 Daltons, and MW_{Rhod} is the molecular weight of the dye, 527.53 Daltons. MR is the molar ratio of dye to protein. A ratio of 10 was used for this labeling.

The dye solution is added to the protein solution and covered with aluminum foil to keep it out of light. The solution is mixed using a rotary shaker for 30 minutes.

Then, the labeled solution needs to be filtered through a PD-10 desalting column (Sephadex G-25M; GE Healthcare) to remove the free dye from the solution. After removing the top cap of the column and pour off the excess liquid, equilibration of the column with 25 ml PBS buffer is required. Labeled solution is added to the column, and then, same amount of buffer is added and the output is discarded. Finally, buffer is eluted and the output flow is collected with the labeled proteins. The solution could be stored at -20˚C or diluted to the needed concentration. In this project, the concentration used was 0.3 mg/ml.

The protein concentration can be calculated by spectrophotometry, by the following equation:

$$C_{BSA} = \frac{[A_{280} - (A_{585} \times K)] \times DF}{\varepsilon} \times MW_{BSA} \quad \text{(A.2)}$$

Where A_{280} and A_{585} are the UV-light absorption of the protein solution at 280 and 585 nm; DF is the dilution factor; ε is the extinction coefficient that for BSA is approximately 43,824 M^{-1} cm^{-1}.

DNA Staining

YOYO-1 was intercalated within the DNA backbone at a ratio of one molecule of dye per five base pairs of DNA (1:5), similarly as described in Shrewsbury *et al* paper [48]. The average molecular weight of the base pair used was 650 grams/bp mole. The DNA was diluted in TE buffer (10 mM tris-HCl, 1 mM EDTA, from Rockland Inc., Gilbertsville, PA). The dye solution was added conjunctly with β-mercaptoethanol, an oxygen scavenger that protect DNA-dye complex from oxygen radicals, at a final concentration of 4% (v/v). The incubation of DNA and the dye occurred at room temperature in the dark and for a minimum of two hours. The final DNA concentration was 0.075 μg/μl.